

High- p_T Hadron Suppression and Jet Quenching

David d'Enterria and Barbara Betz

Abstract In these introductory lectures, we present a broad overview of the physics of hadron and jet production at large transverse momenta in high-energy nucleus–nucleus collisions. Emphasis is put on experimental and theoretical “jet quenching” observables that provide direct information on the (thermo)dynamical properties of hot and dense QCD matter.

1 Introduction

The research programme of high-energy nucleus–nucleus physics is focused on the study of the fundamental theory of the strong interaction – quantum chromodynamics (QCD) – in extreme conditions of temperature, density, and small parton momentum fraction (low- x) – see, e.g., [1] for a recent review. By colliding two heavy nuclei at relativistic energies one expects to form a hot and dense deconfined medium whose collective (colour) dynamics can be studied experimentally. Lattice QCD calculations [2] predict a new form of matter at energy densities (well) above $\varepsilon_{\text{crit}} \approx 1 \text{ GeV}/\text{fm}^3$ consisting of an extended volume of deconfined and bare-mass quarks and gluons: the quark–gluon plasma (QGP) [3–6].

Direct information on the thermodynamical properties (like temperature, energy, or particle densities) and transport properties (such as viscosities, diffusivities, conductivities) of the QGP is commonly obtained by comparing the results for a given observable Φ_{AA} measured in nucleus–nucleus (AA , “QCD medium”) to those measured in proton–proton (pp , “QCD vacuum”) collisions as a function of

D. d'Enterria (✉)
CERN, PH-EP, CH-1211 Geneva 23, Switzerland LNS, MIT, Cambridge, MA 02139-4307, USA,
david.d'enterria@cern.ch

B. Betz
Institut für Theoretische Physik, Johann Wolfgang Goethe-Universität,
Max-von-Laue-Str. 1, 60438 Frankfurt am Main, Germany,
betz@th.physik.uni-frankfurt.de

centre-of-mass (c.m.) energy $\sqrt{s_{NN}}$, transverse momentum p_T , rapidity y , reaction centrality (impact parameter b), and particle type (mass m). Schematically

$$R_{AA}(\sqrt{s_{NN}}, p_T, y, m; b) = \frac{\text{“hot/dense QCD medium”}}{\text{“QCD vacuum”}} \propto \frac{\Phi_{AA}(\sqrt{s_{NN}}, p_T, y, m; b)}{\Phi_{pp}(\sqrt{s}, p_T, y, m)}. \quad (1)$$

Any observed *enhancements* and/or *suppressions* in the $R_{AA}(\sqrt{s_{NN}}, p_T, y, m; b)$ ratios can then be directly linked to the properties of strongly interacting matter after accounting for a realistic hydrodynamical modelling of the space–time evolution of the expanding system of quarks and gluons (globally called partons) produced in the collision.

2 Jet Quenching and Parton Energy Loss in QCD Matter

2.1 Hard Probes of Hot and Dense QCD Matter

Among all available observables in high-energy nuclear collisions, particles with large transverse momentum and/or high mass, $p_T, m \gtrsim 2 \text{ GeV} \gg \Lambda_{\text{QCD}}$ (where $\Lambda_{\text{QCD}} \approx 0.2 \text{ GeV}$ is the QCD scale) constitute very useful tools to “tomographically” study the hottest and densest phases of the reaction (Fig. 1). Indeed, such

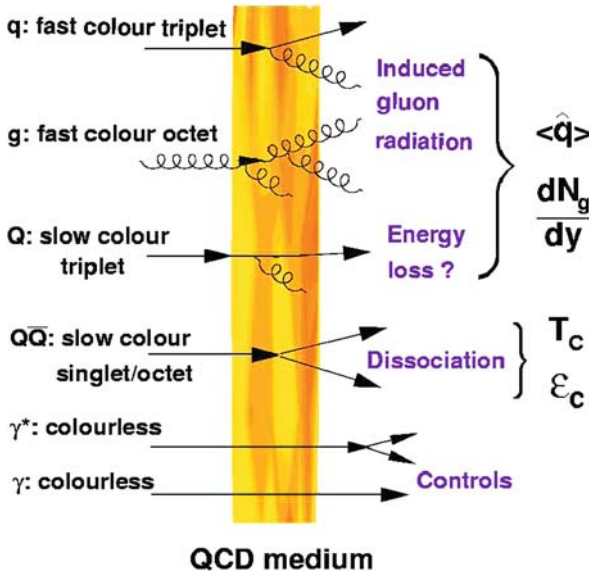


Fig. 1 Examples of hard probes whose modifications in high-energy AA collisions provide direct information on properties of QCD matter such as the transport coefficient \hat{q} , the initial gluon rapidity density dN_g/dy , the critical temperature T_{crit} , and energy density ϵ_{crit} [1]

“hard probes” [7] (i) originate from partonic scatterings with large momentum transfer Q^2 and thus are directly coupled to the fundamental QCD degrees of freedom, (ii) are produced in very short timescales, $\tau \approx 1/p_T \lesssim 0.1$ fm/c, allowing them to propagate through (and be potentially affected by) the medium, and (iii) their cross sections can be theoretically predicted using the perturbative QCD (pQCD) framework.

Jet production in hadronic collisions is an archetypical hard QCD process. An elastic ($2 \rightarrow 2$) or inelastic ($2 \rightarrow 2 + X$) scattering of two partons from each of the colliding hadrons (or nuclei) results in the production of two or more partons in the final state. The two outgoing partons have a large virtuality Q which they reduce by subsequently radiating gluons and/or splitting into quark–antiquark pairs. Such a parton branching evolution is governed by the QCD radiation probabilities given by the Dokshitzer–Gribov–Lipatov–Altarelli–Parisi (DGLAP) equations [8–12] down to virtualities $\mathcal{O}(1 \text{ GeV}^2)$. At this point, the produced partons fragment non-perturbatively into a set of final-state hadrons. The characteristic collimated spray of hadrons resulting from the fragmentation of an outgoing parton is called a “jet”.

One of the first proposed “smoking guns” of QGP formation was “jet quenching” [13], i.e. the attenuation or disappearance of the spray of hadrons resulting from the fragmentation of a parton due to energy loss in the dense plasma produced in the reaction (Fig. 2). The energy lost by a particle in a medium, ΔE , provides fundamental information on its properties. In a general way, ΔE depends both on the particle characteristics (energy E and mass m) and on the plasma properties (temperature T , particle–medium interaction coupling α , and thickness L), i.e.

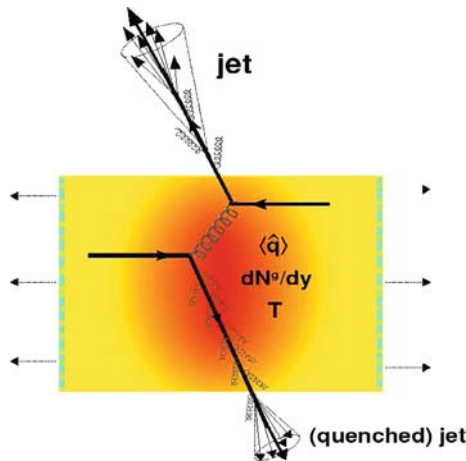


Fig. 2 “Jet quenching” in a head-on nucleus–nucleus collision. Two quarks suffer a hard scattering: one goes out directly to the vacuum, radiates a few gluons, and hadronises; the other goes through the dense plasma formed in the collision (characterised by transport coefficient \hat{q} and gluon density dN^s/dy), suffers energy loss due to medium-induced gluonstrahlung, and finally fragments outside into a (quenched) jet

$\Delta E(E, m, T, \alpha, L)$. The following (closely related) variables are extremely useful to characterise the energy loss in a medium:

- the *mean free path* $\lambda = 1/(\rho\sigma)$, where ρ is the medium density ($\rho \propto T^3$ for an ideal gas) and σ the integrated cross section of the particle–medium interaction,¹
- the *opacity* $N = L/\lambda$ or number of scattering centres in a medium of thickness L ,
- the *Debye mass* $m_D(T) \sim g T$ (where g is the coupling parameter, i.e. $m_D \sim e T$, $\alpha_s^{1/2} T$ in QED, QCD) is the inverse of the screening length of the (chromo) electric fields in the plasma. m_D characterises the lowest momentum exchanges with the medium: the effective masses of the plasma constituents are $\mathcal{O}(m_D)$,
- the *transport coefficient* $\hat{q} \equiv m_D^2/\lambda$ encodes the “scattering power” of the medium through the average transverse momentum squared transferred to the traversing particle per unit path length. \hat{q} combines both thermodynamical (m_D, ρ) and dynamical (σ) properties of the medium [14–16]:

$$\hat{q} \equiv m_D^2/\lambda = m_D^2 \rho \sigma . \quad (2)$$

As a numerical example,² let us consider an equilibrated *gluon* plasma at $T = 0.4$ GeV and a strong coupling $\alpha_s \approx 0.5$ [17]. At this temperature, the particle (energy) density is $\rho_g = 16/\pi^2 \zeta(3) \cdot T^3 \approx 15 \text{ fm}^{-3}$ ($\epsilon_g = 8\pi^2/15 \cdot T^4 \approx 17 \text{ GeV/fm}^3$), i.e. 100 times denser than normal nuclear matter ($\rho = 0.15 \text{ fm}^{-3}$). At leading order (LO), the Debye mass is $m_D = (4\pi\alpha_s)^{1/2} T \approx 1$ GeV. The (transport) gluon–gluon cross section is to LO accuracy: $\sigma_{gg} \simeq 9\pi\alpha_s^2/(2m_D^2) \approx 1.5$ mb. The gluon mean free path in such a medium is $\lambda_g = 1/(\rho_g\sigma_{gg}) \simeq (18/\pi^2 \zeta(3)\alpha_s T)^{-1} \simeq 0.45$ fm (the mean free path for a quark is $\lambda_q = 9/4\lambda_g \approx 1$ fm). The transport coefficient is therefore $\hat{q} \simeq m_D^2/\lambda_g \simeq 2.2 \text{ GeV}^2/\text{fm}$. Note that such a numerical value has been obtained with a LO expression for the parton-medium cross section. Higher order scatterings can well account for a factor $K = 2\text{--}3$ larger \hat{q} .

- the *diffusion constant* D , characterising the dynamics of *heavy* non-relativistic particles (mass M and speed v) traversing the plasma, is connected, via the Einstein relations

$$D = 2T^2/\kappa = T/(M \eta_D) \quad (3)$$

to the *momentum diffusion coefficient* κ – the average momentum gained by the particle per unit time (related to the transport coefficient as $\kappa \approx \hat{q} v$) – and the *momentum drag coefficient* η_D .

¹ One has $\lambda \sim (\alpha T)^{-1}$ since the QED (QCD) Coulomb (Yukawa) scattering is $\sigma_{el} \propto \alpha/T^2$.

² Natural units used ($c = \hbar = 1$). For unit conversion, multiply by powers of $\hbar c = 0.197 \text{ GeV fm}$.

2.2 Mechanisms of In-Medium Energy Loss

In the most general case, the total energy loss of a particle traversing a medium is the sum of collisional and radiative terms: $\Delta E = \Delta E_{\text{coll}} + \Delta E_{\text{rad}}$. Depending on the kinematic region, a (colour) charge can lose energy³ in a plasma with temperature T mainly⁴ by two mechanisms:

- **Collisional energy loss** through *elastic* scatterings with the medium constituents (Fig. 3, left), dominates at low particle momentum. The *average* energy loss in one scattering (with cross section $d\sigma/dt$, where t is the momentum transfer) is

$$\langle \Delta E_{\text{coll}}^{\text{1scat}} \rangle = \frac{1}{\sigma T} \int_{m_D^2}^{t_{\text{max}}} t \frac{d\sigma}{dt} dt . \quad (4)$$

- **Radiative energy loss** through *inelastic* scatterings within the medium (Fig. 3, right) dominates at higher momenta. This loss can be determined from the corresponding single- or double-differential photon/gluon *Bremsstrahlung spectrum* ($\omega dI_{\text{rad}}/d\omega$ or $\omega d^2I_{\text{rad}}/d\omega dk_{\perp}^2$, where ω, k_{\perp} are the energy, transverse momentum of the radiated photon/gluon):

$$\Delta E_{\text{rad}}^{\text{1scat}} = \int^E \omega \frac{dI_{\text{rad}}}{d\omega} d\omega \quad \text{or} \quad \Delta E_{\text{rad}}^{\text{1scat}} = \int^E \int^{k_{T,\text{max}}} \omega \frac{d^2I_{\text{rad}}}{d\omega dk_{\perp}^2} d\omega dk_{\perp}^2 . \quad (5)$$

For incoherent scatterings one has simply $\Delta E^{\text{tot}} = N \cdot \Delta E^{\text{1scat}}$, where $N = L/\lambda$ is the opacity. The energy loss per unit length or *stopping power*⁵ is:

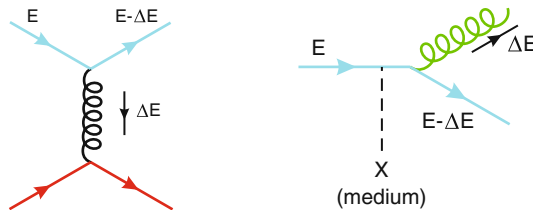


Fig. 3 Diagrams for collisional (*left*) and radiative (*right*) energy losses of a quark of energy E traversing a quark–gluon medium

³ Note that if the energy of the particle is similar to the plasma temperature ($E \approx T$) the particle can also *gain* energy while traversing it.

⁴ In addition, synchrotron-, Čerenkov-, and transition-radiation energy losses can take place, respectively, if the particle interacts with the medium magnetic field, if its velocity is greater than the local phase velocity of light, or if it crosses suddenly from one medium to another. Yet those effects are usually less important in terms of the amount of E_{loss} .

⁵ By “stopping power”, one means a property of the matter, while “energy loss per unit length” describes what happens to the particle. The numerical value and units are identical (and both are usually written with a minus sign in front).

$$-\frac{dE}{dl} = \frac{\langle \Delta E^{\text{tot}} \rangle}{L}, \tag{6}$$

which for incoherent scatterings reduces to $-dE/dl = \langle \Delta E^{\text{1scat}} \rangle / \lambda$. As an example, we show in Fig. 4 the stopping power of muons in copper. At low and high energies, the collisional (aka “Bethe–Bloch”) and the radiative energy losses dominate, respectively.

Yet the hot and dense plasma environment that one encounters in “jet quenching” scenarios is not directly comparable to the QED energy loss in *cold* matter represented in Fig. 4. A recent review by Peigné and Smilga [18] presents the parametric dependences of the energy loss of a lepton traversing a *hot* QED plasma with temperature T and Debye-mass m_D . In a simplified manner, inserting the Coulomb (lepton–lepton) and Compton (lepton–photon) scattering cross sections in Eq. (4) and using Eq. (6), one obtains

- Light lepton ($M^2 \ll ET$): $-\frac{dE_{\text{coll}}}{dl} \approx \frac{\pi}{3} \alpha^2 T^2 \ln \left(\frac{ET}{m_D^2} \right) \approx \frac{\pi}{3} \alpha m_D^2 \ln \left(\frac{ET}{m_D^2} \right)$
- Heavy lepton ($M^2 \gg ET$): $-\frac{dE_{\text{coll}}}{dl} \approx \frac{2\pi}{3} \alpha^2 T^2 \ln \left(\frac{ET}{m_D M} \right) \approx \frac{2\pi}{3} \alpha m_D^2 \ln \left(\frac{ET}{m_D M} \right)$

For *radiative* losses, the amount of photon emission depends chiefly on the thickness of the plasma.⁶ For thin media ($L \ll \lambda$), the traversing particle suffers at most one single scattering and the QED radiation spectrum is just given by the Bethe–Heitler

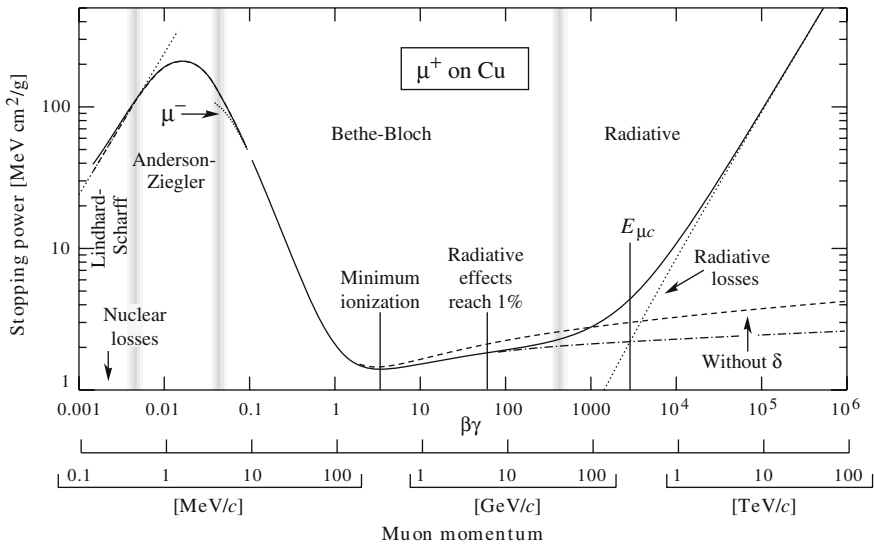


Fig. 4 Stopping power, $-dE/dl$, for positive muons in copper as a function of $\beta\gamma = p/Mc$ (or momentum p). The *solid* curve indicates the total stopping power [19]

⁶ We consider here the formulas where the charged particle is produced *inside* the plasma, as this is the typical situation encountered in a QGP.

(BH) Bremsstrahlung expression. On the contrary, for thick media ($L \gg \lambda$) there are N (=opacity) scatterings and the Landau–Pomeranchuk–Migdal (LPM) [20] coherence effect⁷ reduces the amount of radiation compared to N times the BH spectrum. Making use of Eq. (5) one can obtain [18]:

- BH photon spectrum ($L \ll \lambda$)⁸: $\omega \frac{dI_{\text{rad}}}{d\omega} \approx \alpha (L^2 m_D^2 / \lambda) \cdot \omega / E^2 \approx \alpha \hat{q} L \cdot \omega / E^2$

$$\Delta E_{\text{rad}}^{\text{BH}} \approx \alpha \hat{q} L^2 \approx \alpha^3 T^3 L^2 \implies -\frac{dE_{\text{rad}}}{dl} = \frac{\Delta E_{\text{rad}}}{L} \approx \alpha^3 T^3 L. \quad (7)$$

- LPM photon spectrum ($L \gg \lambda$): $\omega \frac{dI_{\text{rad}}}{d\omega} \approx \alpha^2 L \sqrt{T^3 \frac{\omega}{E^2} \ln(E^2 / (\omega T))}$

$$\Delta E_{\text{rad}}^{\text{LPM}} \approx \alpha^2 L \sqrt{ET^3 \ln(E/T)} \implies -\frac{dE_{\text{rad}}}{dl} \approx \alpha^2 \sqrt{ET^3 \ln(E/T)}. \quad (8)$$

In general, the radiative energy losses of an energetic lepton crossing a hot QED plasma are much larger than their collisional losses. Yet, if the particle is heavy, the amount of radiation at angles within a cone $\theta < M/E$ is suppressed by a factor m_D^2/M^2 (“dead cone” effect, see later) resulting in a reduction of the Bremsstrahlung emission by a factor $m_D^2/M^2 = \alpha T^2/M^2$.

The main differences from QED and QCD result from the non-Abelian nature of QCD: the fact that gluons can also interact with themselves (at variance with photons in QED) introduces several important changes. First, the QCD coupling α_s runs more rapidly than α_{em} (at least for not asymptotically high temperatures), and the scale Q at which $\alpha_s(Q)$ is evaluated needs to be explicitly considered in all calculations of *collisional* energy losses [21, 22]. Second, for *radiative* losses it is crucial to take into account the different couplings between quarks and gluons. The relative strengths of the three distinct QCD vertices, $\alpha_s C_F$ for $q \rightarrow qg$, $\alpha_s C_A$ for $g \rightarrow gg$, and $\alpha_s T_F$ for $g \rightarrow q\bar{q}$, are completely determined by the structure (Casimir factors C_R) of the gauge group describing the strong force [23]. For $SU(N_c)$ where N_c is the number of colours, $C_A = N_c$, $C_F = (N_c^2 - 1)/2N_c$, and $T_F = 1/2$. The probability for a gluon (quark) to radiate a gluon is proportional to the colour factor $C_A = 3$ ($C_F = 4/3$). In the asymptotic limit, and neglecting the gluon splitting into quark–antiquark pairs (proportional to the smaller factor $T_R = 1/2$), the average number of gluons radiated by a gluon is $C_A/C_F = 9/4$ times higher than that radiated by a quark. That is the reason why gluon jets have a larger (and softer) hadron multiplicity than quark jets.

⁷ The LPM effect describes the fact that, since it takes a finite time to emit a photon, neighbouring scattering centres interfere coherently and act as one effective scattering centre, inducing *single* photon radiation.

⁸ This spectrum is often written as $\omega \frac{dI_{\text{rad}}}{d\omega} \approx \alpha \omega_c \omega / E^2$, where $\omega_c \approx \hat{q} L^2$ is the characteristic frequency of the radiated photons.

2.2.1 QCD Collisional Energy Loss

The collisional energy loss due to elastic scattering of a parton of energy E inside a QGP of temperature T was originally estimated by Bjorken [13] and Braaten–Thoma [24] and later improved (including running coupling, finite energy kinematics, and quark mass effects) by various authors [21, 22, 25]. Using Eq. (4) with the momentum-transfer integral limits given by (i) the QGP Debye mass squared $t_{\min} = m_D^2(T) \simeq 4\pi\alpha_s T^2(1 + N_f/6)$ and (ii) $t_{\max} = s \simeq ET$ and taking the dominant contribution to the parton–parton t -differential elastic cross section

$$\frac{d\sigma}{dt} \approx C_i \frac{4\pi\alpha_s^2(t)}{t^2}, \quad \text{with } \alpha_s(t) = \frac{12\pi}{(33 - 2n_f) \ln(t/\Lambda_{\text{QCD}}^2)}, \quad (9)$$

where $C_i = 9/4, 1, 4/9$ are the colour factors for $gg, gq,$ and qq scatterings respectively, one finally obtains [22]

- Light quark, gluon: $-\frac{dE_{\text{coll}}}{dl}\Big|_{q,g} = \frac{1}{4} C_R \alpha_s(ET) m_D^2 \ln\left(\frac{ET}{m_D^2}\right),$
- Heavy quark: $-\frac{dE_{\text{coll}}}{dl}\Big|_Q = -\frac{dE_{\text{coll}}}{dl}\Big|_q - \frac{2}{9} C_R \pi T^2 [\alpha_s(M^2)\alpha_s(ET) \ln\left(\frac{ET}{M^2}\right)],$

with $C_R = 4/3$ (3) being the quark (gluon) colour charge. The amount of ΔE_{coll} is linear with the medium thickness, and it depends only logarithmically on the initial parton energy. As a numerical example, taking $T = 0.4$ GeV, $E = 20$ GeV, $M = 1.3$ GeV (charm quark), and $\alpha_s = 0.5$ (which yields $m_D = 1$ GeV), the elastic energy loss per unit length is $-dE_{\text{coll}}/dl\Big|_q = 2.3$ GeV/fm and $-dE_{\text{coll}}/dl\Big|_Q = 2.6$ GeV/fm.

2.2.2 QCD Radiative Energy Loss

The dominant mechanism of energy loss of a fast parton in a QCD environment is of radiative nature (“gluonstrahlung”) [26–32]: a parton traversing a QGP loses energy mainly by medium-induced multiple gluon emission. The radiated gluon spectrum, $\omega dI(\omega, l)/d\omega$, has been computed by diverse groups under various approximations (see Sect. 3.2). The starting point is the QCD radiation probabilities given by DGLAP splitting functions ($P_{q,g \rightarrow g}$): $\omega dI(\omega)/d\omega \propto P_{q,g \rightarrow g}(\omega/E)$, modified to take into account the enhanced medium-induced radiation. All medium modifications are often encoded into the “transport coefficient” parameter, \hat{q} , introduced previously, Eq. (2). For thin (thick) media, one deals with the Bethe–Heitler (Landau–Pomeranchuk–Migdal) gluonstrahlung spectrum. In the LPM case, one further differentiates between the soft and hard gluon emission cases with respect to the characteristic gluonstrahlung energy⁹ $\omega_c = \frac{1}{2}\hat{q} L^2$. Making use of Eq. (5), the basic QCD radiative energy loss formulas read [12]

⁹ Up to prefactors, ω_c is the average energy lost in the medium: $\omega_c \simeq 2 \langle \Delta E_{\text{rad}} \rangle / (\alpha_s C_R)$.

- Bethe–Heitler (BH) regime ($L \ll \lambda$):

$$\omega \frac{dI_{\text{rad}}}{d\omega} \approx \alpha_s C_R \hat{q} L^2 / \omega \implies \Delta E_{\text{rad}}^{\text{BH}} \approx \alpha_s C_R \hat{q} L^2 \ln(E/(m_D^2 L)). \quad (10)$$

- Landau–Pomeranchuk–Migdal (LPM) regime ($L \gg \lambda$):

$$\omega \frac{dI_{\text{rad}}}{d\omega} \approx \alpha_s C_R \begin{cases} \sqrt{\hat{q} L^2 / \omega} \\ \hat{q} L^2 / \omega \end{cases} \implies \Delta E_{\text{rad}}^{\text{LPM}} \approx \alpha_s C_R \begin{cases} \hat{q} L^2 & (\omega < \omega_c) \\ \hat{q} L^2 \ln(E/(\hat{q} L^2)) & (\omega > \omega_c). \end{cases} \quad (11)$$

The main differences between the energy loss in a QCD and QED plasma are the colour factors (C_R) and the extra logarithmic dependence of ΔE_{rad} on the energy E of the traversing particle. As a numerical example, taking $E = 20$ GeV, $L = 6$ fm, and a medium with $\hat{q} = 2$ GeV²/fm, the LPM radiative energy losses per unit length dE_{rad}/dl are $\mathcal{O}(10$ GeV/fm), to be compared with the elastic losses of $\mathcal{O}(2$ GeV/fm) estimated before. As we see in Fig. 5, ΔE_{coll} is in general a small correction compared to ΔE_{rad} for light quarks and gluons but it can be an important contribution for slower heavy quarks (see next).

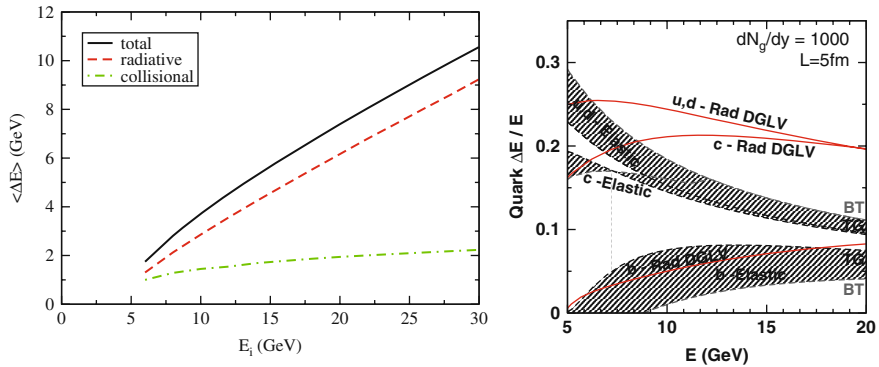


Fig. 5 Comparison of the average radiative and elastic energy losses of light quarks (*left*) and light and heavy quarks (*right*) passing through the medium produced in central AuAu collisions at RHIC energies as obtained by the AMY [34] and DGLV [35] models (see later)

2.2.3 Heavy-Quark Radiative Energy Loss (“Dead Cone” Effect)

Gluon bremsstrahlung off a heavy quark differs from that of a massless parton. Due to kinematics constraints, the radiation is suppressed at angles smaller than the ratio of the quark mass M to its energy E . The double-differential distribution of gluons of transverse momentum k_{\perp} and energy ω radiated by a heavy quark at small angles ($k_{\perp} \approx \omega \theta$) differs from the standard bremsstrahlung spectrum by the factor

$$\omega \frac{dI_{\text{rad},Q}}{d\omega dk_{\perp}^2} = \frac{\alpha_s C_F}{\pi} \frac{k_{\perp}^2}{(k_{\perp}^2 + \omega^2 \theta_0^2)^2} \approx \omega \frac{dI_{\text{rad}}}{d\omega dk_{\perp}^2} \cdot \left(1 + \frac{\theta_0^2}{\theta^2}\right)^{-2}, \quad \theta_0 \equiv \frac{M}{E} = \frac{1}{\gamma}. \quad (12)$$

This effect, known as the “dead cone” [33], results in a reduction of the total gluon radiation emitted off heavy quarks. In the medium, the total amount of reduction depends on a non-trivial way on the various kinematics scales (E , M , L) of the problem [18]. In a simplified way, the reduction is $\mathcal{O}(m_D/M)$ (compared to $\mathcal{O}(m_D^2/M^2)$ in the QED case). For a plasma with Debye mass $m_D = 1 \text{ GeV}/c^2$, the reduction of radiative energy loss for a charm (bottom) quark of mass 1.3 (4.2) GeV/c^2 is a factor $\sim 25\%$ (75%).

2.3 Phenomenological Consequences of Parton Energy Loss

Medium-induced parton energy loss in AA reactions results in various observable experimental consequences compared to the same measurements in proton–proton (pp) collisions in “free space”. The presence of jet quenching manifests itself via

- (i) a suppression of the spectrum (dN_{AA}/dp_T) of high- p_T hadrons [26, 27],
- (ii) unbalanced back-to-back high- p_T di-hadron azimuthal correlations ($dN_{\text{pair}}/d\phi$) [36, 37],
- (iii) modified energy–particle flow (softer hadron spectra, larger multiplicity, increased angular broadening, etc.) within the final jets [38–43].

Due to the aforementioned hierarchy of flavour-dependent radiative energy losses

$$\Delta E_{\text{rad}}(g) > \Delta E_{\text{rad}}(q) > \Delta E_{\text{rad}}(c) > \Delta E_{\text{rad}}(b), \quad (13)$$

all these medium effects are expected to be larger for gluons and u , d , s quarks than for c or b quarks (the top quark decays into $W b$ immediately, $\tau < 0.1 \text{ fm}/c$, after production).

- (i) High- p_T leading hadron spectra

The *leading hadron* of a jet is the hadron that carries the largest fraction of the energy of the fragmenting parton.¹⁰ In a heavy-ion collision, if the parent parton suffers energy loss, the energy available for such hadrons is reduced and consequently their spectrum is depleted compared to pp . From the measured suppression factor one can determine ΔE_{loss} and estimate properties of the produced plasma (expanding with original transverse area $A_{\perp} = \pi R_A^2 \approx 150 \text{ fm}^2$ and thickness L) such as

¹⁰ The high- p_T part of hadron spectra is dominated by particles with $\langle z \rangle = p_{\text{hadron}}/p_{\text{parton}} \approx 0.4\text{--}0.7$ [43].

- the average *transport coefficient* $\langle \hat{q} \rangle$, from Eq. (10): $\langle \Delta E \rangle \propto \alpha_s C_R \langle \hat{q} \rangle L^2$,
- the initial *gluon density* dN^g/dy from [30, 31]:

$$\Delta E \propto \alpha_s^3 C_R \frac{1}{A_\perp} \frac{dN^g}{dy} L. \quad (14)$$

(ii) High- p_T di-hadron correlations

Parton–parton $2 \rightarrow 2$ scatterings are balanced in p_T , i.e. they are back-to-back in azimuthal angle ($\Delta\phi \approx \pi$). Such azimuthal correlation is smeared out if one or both partons suffer rescatterings in a dense plasma.

- The φ -broadening arising from the interactions of a parton in an expanding QGP $\langle k_T^2 \rangle_{\text{med}} \propto m_D^2/\lambda \ln(L/\tau_0)$, is $\langle k_T^2 \rangle_\varphi = \langle k_T^2 \rangle_{\varphi, \text{vac}} + \frac{1}{2} \langle k_T^2 \rangle_{\text{med}}$. The azimuthal correlations between the hadrons issuing from quenched partons will show a dependence on the \hat{q} and thickness of the medium: $d^2 N_{\text{pair}}/d\Delta\phi = f(\hat{q}, L)$.

In addition, it has been proposed that a fast parton propagating through a QGP with supersonic ($\beta > c_s$) or “superluminal” ($\beta > 1/n$) velocities can generate a wake of lower energy gluons with either Mach- [44–48] or Čerenkov-like [48–51] conical angular patterns. After hadronisation those secondary gluons can show up in the final azimuthal correlations of the measured hadrons with respect to the original jet axis:

- In the first case, the *speed of sound* of the traversed matter, ¹¹ $c_s^2 = \partial P/\partial \varepsilon$, can be determined from the characteristic Mach angle θ_M of the secondary hadrons:

$$\cos(\theta_M) = \frac{c_s}{\beta}. \quad (15)$$

- In the second scenario, the *refractive index* of the medium, $n \approx \sqrt{\varepsilon_r}$ where ε_r is the gluon dielectric constant, can be estimated from the Čerenkov angle of emission θ_c of the hadrons:

$$\cos(\theta_c) = \frac{1}{n\beta} = \frac{1}{\sqrt{\varepsilon_r}\beta}. \quad (16)$$

(iii) Jet spectra and jet shapes

The measurements of fully reconstructed (di)jets or of jets tagged by an away-side photon or Z -boson [52, 53] in heavy-ion collisions allow one to investigate the mechanisms of in-medium parton radiation and to characterise the medium properties via

¹¹ The speed of sound – namely the speed of a small disturbance through the medium – for an *ideal* QGP (with $\varepsilon = 3P$, where P is the pressure) is simply $c_s = 1/\sqrt{3}$.

- Medium-modified jet profiles and multiplicities [38, 54], through the differential $\rho^{\text{med}}(r; \hat{q})$ and integrated $\Psi^{\text{med}}(r; \hat{q})$ jet shapes, which provide a sensitive probe of the mechanisms of energy loss in a QCD plasma.
- Medium-modified fragmentation functions [55], $D_{\text{parton} \rightarrow \text{hadron}}^{\text{med}}(z)$ where $z = p_{\text{hadron}}/p_{\text{parton}}$ is the fractional energy carried by a hadron in the jet, are a sensitive probe of the plasma properties (\hat{q} for a given L) [39, 56, 57, 40]. Medium effects enter, e.g. as an additive correction to the DGLAP splitting functions:

$$P_{\text{med}}(z) = P_{\text{vac}}(z) + \Delta P(z, Q^2, E; \hat{q}, L), \quad (17)$$

where $\Delta P(z, Q^2) \simeq 2\pi Q^2/\alpha_s dI_{\text{rad}}(\hat{q}, L)/dzdQ^2$ is directly derivable from the medium-induced gluon radiation spectrum, Eq. (11).

3 Parton Energy Loss Phenomenology

The use of fast partons as a calibrated tomographic probes of hot and dense QCD matter in heavy-ion collisions relies on the possibility to compute theoretically (i) their perturbative production cross sections and (ii) their modifications suffered while propagating through a strongly interacting medium. We discuss here the basic pQCD principles used to compute high- p_T hadron (and jet) cross sections, and we outline the various existing parton energy loss schemes.

3.1 High- p_T Hadroproduction: QCD Factorisation in AA Collisions

Because of asymptotic freedom, the QCD coupling α_s is small for high-energy (short distance) parton interactions: $\alpha_s(Q^2 \rightarrow \infty) \rightarrow 0$. The single inclusive¹² production of a high- p_T parton c in a parton–parton collision, $ab \rightarrow c + X$, can be thus computed using perturbation theory techniques. Over short distances, the infinite number of Feynman diagrams that would theoretically result in the production of the outgoing parton c can be approximated accurately by a much more manageable number of terms. In high-energy *hadron–hadron* collisions, the production of high- p_T particles can be computed from the underlying *parton–parton* processes using the QCD “factorisation theorem” [58]. The production cross section of a high- p_T hadron h can be written, to order $\mathcal{O}(1/Q^2)$, as the product

$$d\sigma_{AB \rightarrow h}^{\text{hard}} = f_{a/A}(x_1, Q^2) \otimes f_{b/B}(x_2, Q^2) \otimes d\sigma_{ab \rightarrow c}^{\text{hard}}(x_1, x_2, Q^2) \otimes D_{c \rightarrow h}(z, Q^2), \quad (18)$$

where $\sigma_{ab \rightarrow c}(x_1, x_2, Q^2)$ is the perturbative partonic cross section computable up to a given order in α_s , and there are two non-perturbative terms:

¹² *Inclusive* refers to the consideration of *all* possible channels that result in the production of a given particle c , without any particular selection of the final state X .

- $f_{a/A}(x, Q^2)$: parton distribution functions (PDF), encoding the probability of finding a parton of flavour a and momentum fraction $x = p_{\text{parton}}/p_{\text{nucleus}}$ inside the nucleus A ,
- $D_{c \rightarrow h}(z, Q^2)$: fragmentation function (FF), describing the probability that the outgoing parton c fragments into the observed hadron h with fractional momentum $z = p_{\text{hadron}}/p_{\text{parton}}$,

that are universal objects that can be determined experimentally, e.g. in deep-inelastic e^\pm nucleus and e^+e^- collisions, respectively. In Eq. (18), one sets $D_{c \rightarrow h} = \delta(1 - z)$ if interested in the total parton (i.e. jet) cross section.

The basic assumption underlying the factorised form of Eq. (18) is that the characteristic time of the parton–parton interaction is much shorter than any long-distance interaction occurring before (among partons belonging to the same PDF) or after (during the evolution of the struck partons into their hadronic final state) the hard collision itself (see sketch in Fig. 6). The validity of Eq. (18) holds thus on the possibility to separate long- and short-distance effects with independent QCD time- (length-) scales, as well as on the “leading-twist”¹³ assumption of *incoherent* parton–parton scatterings. Since partons are effectively “frozen” during the hard scattering, one can treat each nucleus as a collection of free partons. Thus, *with regard to high- p_T production*, the density of partons in a nucleus with mass number A is expected to be simply equivalent to that of a superposition of A independent nucleons: $f_{a/A}(x, Q^2) = A \cdot f_{a/N}(x, Q^2)$. Thus,

$$d\sigma_{AB \rightarrow h}^{\text{hard}} \approx A \cdot B \cdot f_{a/p}(x, Q^2) \otimes f_{b/p}(x, Q^2) \otimes d\sigma_{ab \rightarrow c}^{\text{hard}} \otimes D_{c \rightarrow h}(z, Q^2). \quad (19)$$

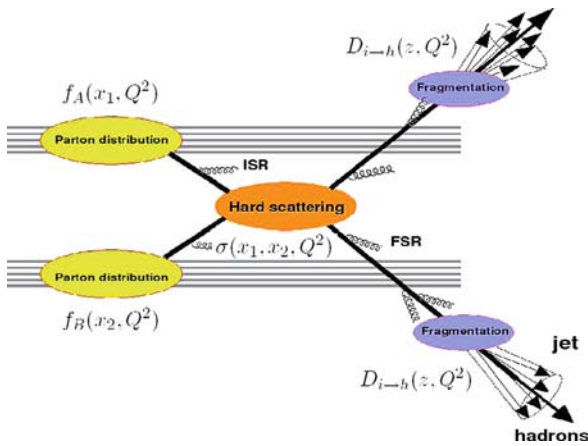


Fig. 6 Sketch of dijet production and pQCD factorisation in hadronic collisions

¹³ Processes in which more than one parton from the same hadron/nucleus interact coherently, are called “higher twist” processes.

From (18), it is clear that QCD factorisation implies that total hard inclusive cross sections in a AB reaction scale simply as $A \cdot B$ times the corresponding pp cross sections:

$$d\sigma_{AB}^{\text{hard}} = A \cdot B \cdot d\sigma_{pp}^{\text{hard}}. \quad (20)$$

Since nucleus–nucleus experiments usually measure invariant *yields* for a given centrality bin (or impact parameter b), one writes instead

$$dN_{AB}^{\text{hard}}(b) = \langle T_{AB}(b) \rangle \cdot d\sigma_{pp}^{\text{hard}}, \quad (21)$$

where the nuclear overlap function at b , $T_{AB}(b)$, is determined within a geometric Glauber eikonal model from the measured Woods–Saxon distribution for the interacting nuclei [59]. Intuitively, one can think of the nuclear overlap $T_{AA}(b)$ as a function that characterises the surface profile of two “beams” of nucleons colliding at a distance b . The [area] $^{-1}$ units of T_{AA} indicate that it represents somehow the effective “parton (integrated) luminosity” of the collision. Since the number of inelastic nucleon–nucleon (NN) collisions at b , $N_{\text{coll}}(b)$, is proportional to $T_{AB}(b)$: $N_{\text{coll}}(b) = T_{AB}(b) \cdot \sigma_{NN}^{\text{inel}}$, one also writes often Eq. (21) as

$$dN_{AB}^{\text{hard}}(b) = \langle N_{\text{coll}}(b) \rangle \cdot dN_{pp}^{\text{hard}}. \quad (22)$$

For minimum-bias¹⁴ AB collisions, the average nuclear overlap and number of NN collisions take a simple form¹⁵: $\langle T_{AB} \rangle = AB / \sigma_{AB}^{\text{geo}}$ and $\langle N_{\text{coll}} \rangle = AB \cdot \sigma_{NN} / \sigma_{AB}^{\text{geo}}$. The standard method to quantify the effects of the medium on the yield of a hard probe in a AA reaction is thus given by the *nuclear modification factor*:

$$R_{AA}(p_T, y; b) = \frac{d^2 N_{AA} / dy dp_T}{\langle T_{AA}(b) \rangle \times d^2 \sigma_{pp} / dy dp_T}. \quad (23)$$

This factor, which is a quantitative version of the ratio (1), measures the deviation of AA at b from an incoherent superposition of NN collisions ($R_{AA} = 1$). This normalisation is often known as “binary collision scaling”.

3.2 Jet Quenching Models

The energy loss formulas presented in Sect. 2.2 refer to an idealistic situation with an infinite-energy parton traversing a *static* and *uniform* QGP with an ideal-gas

¹⁴ *Minimum-bias* collisions are those where there is no specific selection of the final state (e.g. in particular no centrality selection for heavy ions).

¹⁵ For example, for AuAu at $\sqrt{s_{NN}} = 200$ GeV ($\sigma_{NN}^{\text{inel}} = 41$ mb, $\sigma_{\text{AuAu}}^{\text{geo}} = 7000$ mb): $\langle T_{\text{AuAu}} \rangle = 5.5$ (23.3) mb^{-1} and $\langle N_{\text{coll}} \rangle = 230$ (955) for minimum-bias (0–10% most central) collisions, respectively.

equation-of-state (EoS). Experimentally, the situation that one encounters with *realistic* plasmas in heavy-ion collisions is more complex:

- first, there is no direct measurement of the traversing parton but (in the best case) only of the final-state *hadrons* issuing from its fragmentation,
- the traversing partons can be produced at any point of the fireball and their energy spectrum is steeply (power law) falling,
- the temperature and density of the plasma, and correspondingly its Debye mass and transport coefficient, are position dependent: $m_D(\mathbf{r}), \hat{q}(\mathbf{r})$,
- the produced plasma is expanding with large longitudinal (transversal) velocities, $\beta \approx 1$ (0.7),
- the finite size of the plasma and associated energy loss fluctuations have to be taken into account.

All those effects can result in potentially significant deviations from the analytical formulas of Sect. 2.2 (e.g. in an expanding plasma the dependence of ΔE_{rad} on the medium thickness L becomes effectively *linear* rather than quadratic). Four major phenomenological approaches have been developed [60] to connect the QCD energy loss calculations with the experimental observables mentioned in Sect. 2.3:

- Path-integral approach to the opacity expansion (BDMPS–LCPI/ASW) [61–67, 32, 68, 69]
- Reaction operator approach to the opacity expansion (DGLV) [70–73, 35]
- Higher twist (HT) [74–79]
- Finite temperature field theory approach (AMY) [80–83]

The models differ in their assumptions about the relationships between the relevant scales (parton energy E and virtuality Q^2 , and medium typical momentum $\mu \approx m_D$ and spatial extent L), as well as by how they treat or approximate the structure of the medium. In practical terms, all schemes are based on a pQCD factorised approach, i.e. on Eq. (18), where the *entire* effect of energy loss is concentrated on the calculation of the medium-modified parton fragmentation functions into final hadrons: $D_{c \rightarrow h}^{\text{vac}}(z) \rightarrow D_{c \rightarrow h}^{\text{med}}(z', \hat{q})$. The final hadronisation of the hard parton is always assumed to occur in the vacuum after the parton, with degraded energy ($z' < z$), has escaped from the medium (Fig. 7).



Fig. 7 Schematic representation of parton energy loss implemented via energy rescaling of the fragmentation function [55]

3.2.1 BDMPS–LCPI and ASW

The approaches of Baier, Dokshitzer, Müller, Peigné, and Schiffer (BDMPS) [65, 66, 84, 85] and the light-cone path integral (LCPI) by Zakharov [61] compute

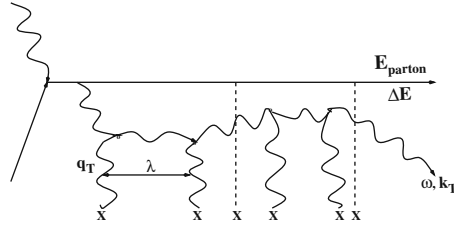


Fig. 8 Typical gluon radiation diagram in the BDMPS approach [66]

energy loss in a coloured medium in a multiple soft-scatterings approximation. A hard parton traversing the medium interacts with various scattering centres and splits into an outgoing parton as well as a radiated gluon (Fig. 8). The propagation of the traversing parton and radiated gluons is expressed using Green's functions which are obtained by a path integral over the fields. The final outcome of the approach is a complex analytical expression for the radiated gluon energy distribution $\omega dI/d\omega$ as a function of the transport coefficient \hat{q} defined perturbatively as [86]

$$\hat{q} \equiv \rho \int d^2k_{\perp} k_{\perp}^2 \frac{d\sigma}{d^2k_{\perp}}. \quad (24)$$

Here ρ is the density of scattering centres (mainly gluons) in the medium, k_{\perp} is the transverse momentum of the radiated gluon, and $d\sigma$ is the differential parton-medium cross section. The medium-modified parton-to-hadron fragmentation functions are modelled as

$$D_{i \rightarrow h}^{\text{med}}(z', Q^2) = P_E(\varepsilon; \hat{q}) \otimes D_{i \rightarrow h}^{\text{vac}}(z, Q^2), \quad (25)$$

where the *quenching weights* $P_E(\varepsilon; \hat{q})$ – computed by Armesto, Salgado, and Wiedemann (ASW) [32, 87, 69, 88] – encode the probability (assumed Poissonian) that the propagating parton loses a fraction of energy $\varepsilon = \Delta E/E$ due to gluon emission in N (=opacity) scatterings

$$P_E(\varepsilon; \hat{q}) = \sum_{N=0}^{\infty} \frac{1}{N!} \left[\prod_{i=1}^N \int d\omega_i \frac{dI^{\text{med}}(\hat{q})}{d\omega} \right] \delta \left(\varepsilon; - \sum_{i=1}^N \frac{\omega_i}{E} \right) \exp \left[- \int d\omega \frac{dI^{\text{med}}}{d\omega} \right]. \quad (26)$$

The quenching weights have been implemented in a Monte Carlo model, the parton quenching model (PQM) [89, 90] accounting for a realistic description of the parton production points in heavy-ion collisions. The transport coefficient \hat{q} is used as the fit parameter for the data. The longitudinal expansion of the plasma is taken into account by rescaling the transport coefficient according to the following law [68]:

$$\langle \hat{q} \rangle = \frac{2}{L^2} \int_{\tau_0}^{\tau_0+L} d\tau (\tau - \tau_0) \hat{q}(\tau), \quad (27)$$

where $\hat{q}(\tau) = \hat{q}(\tau_0) (\tau_0/\tau)^\alpha$ and α characterises the time dependence of the plasma density: $n(\tau) \propto \tau^{-\alpha}$. A purely longitudinal (or Bjorken) expansion corresponds to $\alpha = 1$ and is often assumed in phenomenological applications. When $\tau_0 \ll L$, Eq. (27) reduces to $\langle \hat{q} \rangle \simeq 2 \hat{q}(\tau_0) \tau_0/L$ [86].

3.2.2 GLV

The Gyulassy–Levai–Vitev (GLV) [91, 70, 92, 71, 72] (aka DGLV [73, 35]) approach calculates the parton energy loss in a dense deconfined medium consisting, as in the BDMPS approach, of almost static (i.e. heavy) scattering centres (Fig. 9) producing a screened Yukawa potential. At variance with the BDMPS *multiple-soft* bremsstrahlung, GLV starts from the *single-hard* radiation spectrum which is then expanded to account for gluon emission from multiple scatterings via a recursive diagrammatic procedure [71]. The traversing parton gains a transverse momentum \mathbf{q}_\perp and radiates (before or after the scattering) a gluon with a certain momentum $\mathbf{k} = (xE, \frac{k_\perp^2}{xE} \mathbf{k}_\perp)$. The gluon differential distribution at first order in opacity [70] is

$$x \frac{dI^{(1)}}{dx dk_\perp^2} = x \frac{dI^{(0)}}{dx dk_\perp^2} \frac{L}{\lambda_g} \int_0^{q_{\max}^2} d^2q_\perp \frac{\mu_D^2}{\pi(q_\perp^2 + \mu_D^2)^2} \frac{2\mathbf{k}_\perp \cdot \mathbf{q}_\perp (k - q_\perp)^2 L^2}{16x^2 E^2 + (k - q_\perp)_\perp^2 L^2}, \quad (28)$$

where λ_g is the mean free path of the radiated gluon. Applying the aforementioned recursive procedure, one obtains the gluon distribution to finite order ($N \geq 1$) in opacity. Each emission at a given opacity is assumed independent and a probabilistic scheme is set up, wherein, the parton loses an energy fraction ϵ in N tries with a Poisson distribution [72],

$$P_N(\epsilon, E) = \frac{e^{-(N\epsilon)}}{N!} \prod_{i=1}^N \left[\int dx_i \frac{dN^g}{dx_i} \right] \delta \left(\epsilon - \sum_{i=1}^n x_i \right), \quad (29)$$

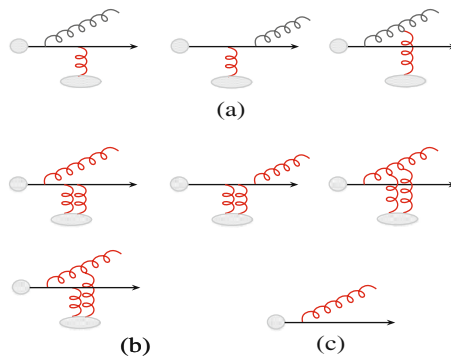


Fig. 9 Diagrams contributing to the lowest order in the opacity energy loss expansion [93]

where $\langle N^g \rangle$ is the mean number of gluons radiated per coherent interaction set. Summing over N gives the probability $P(\varepsilon)$ for an incident parton to lose a momentum fraction ε due to its passage through the medium. This is then used to model a medium-modified FF, by shifting the energy fraction available to produce a hadron in a similar way as Eq. (25). The key medium property to be obtained from the fits to the experimental data is the initial gluon density dN^g/dy , after accounting for longitudinal expansion. Note that the density of colour charges of a cylinder of plasma with “length” τ and surface A_\perp is $\rho \approx dN^g/dy/(\tau A_\perp)$.

3.2.3 Higher Twist (HT)

The higher twist approximation [94–96, 74–76] describes the multiple scattering of a parton as power corrections to the leading-twist cross section (Fig. 10). These corrections are enhanced by the medium length L and suppressed by the power of the hard scale Q^2 . Originally, this approach was applied to calculate the medium corrections to the total cross section in nuclear deep-inelastic eA scattering.

The scheme allows one to compute multiple Feynman diagrams such as those in Fig. 10 which are then combined coherently to calculate the modification of the fragmentation function directly as a medium-dependent *additive* contribution, $D_{i \rightarrow h}^{\text{med}} = D_{i \rightarrow h}^{\text{vac}} + \Delta D_{i \rightarrow h}^{\text{med}}$,

$$\Delta D_{i \rightarrow h}^{\text{med}}(z, Q^2) = \int_0^{Q^2} \frac{dk_\perp^2}{k_\perp^2} \frac{\alpha_s}{2\pi} \left[\int_{z_h}^1 \frac{dx}{x} \sum_{j=q,g} \left\{ \Delta P_{i \rightarrow j}^{\text{med}} D_{j \rightarrow h} \left(\frac{z_h}{x} \right) \right\} \right]. \quad (30)$$

Here, $\Delta P_{i \rightarrow j} \propto P_{i \rightarrow j} C_A \alpha_s T_{qg}^A$ represents the medium-modified splitting function of parton i into j (a momentum fraction x is left in parton j and the radiated gluon or quark carries away a transverse momentum k_\perp). The entire medium effects are incorporated in the nuclear quark–gluon correlation T_{qg}^A term. The normalisation C of this correlator is set by fitting to one data point from which one can directly calculate the medium-modified FFs and then the final hadron spectrum. The parameter C can also be used to calculate the average energy loss suffered by the parton.

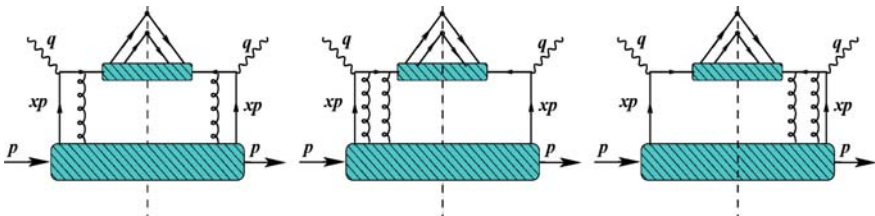


Fig. 10 Leading and next-to-leading order twist contribution to quark scattering in a medium (hatched area) [97]

3.2.4 AMY

The Arnold–Moore–Yaffe (AMY) [80, 98, 99, 82, 83] approach describes parton energy loss in a hot equilibrated QGP, where the hierarchy $T \gg gT \gg g^2T$ can be introduced. The hard parton scatters off other partons in the medium, leading to momentum transfers of $\mathcal{O}(gT)$ and inducing collinear radiation. Multiple scatterings of the incoming (outgoing) parton and the radiated gluon are combined to get the leading-order gluon radiation rate. One essentially calculates the imaginary parts of ladder diagrams such as those shown in Fig. 11 by means of integral equations which yield the $1 \rightarrow 2$ transition rates Γ_{bg}^a of a hard parton (a) into a radiated gluon g and another parton (b). These rates, with T -dependent Bose (for gluons) and Fermi (for quarks) exponential factors for the medium partons, are then used to evolve the original distributions over the medium length by means of a Fokker–Planck-like equation [82]:

$$\frac{dP_a(p)}{dt} = \int dk \sum_{b,c} \left[P_b(p+k) \frac{d\Gamma_{ac}^b(p+k, p)}{dkdt} - P_a(p) \frac{d\Gamma_{bc}^a(p, k)}{dkdt} \right]. \quad (31)$$

The medium-modified FF is obtained from the convolution of the vacuum FF with the hard parton distributions when exiting the plasma [83]:

$$D_{a \rightarrow h}^{\text{med}}(z) = \int dp_f \frac{z'}{z} \sum_a P_a(p_f; p_i) D_{a \rightarrow h}^{\text{vac}}(z'), \quad (32)$$

where $z = p_h/p_i$ and $z' = p_h/p_f$, with p_i and p_f the momenta of the hard partons immediately after the hard scattering and prior to exit from the medium. The model of the medium is essentially contained in the space–time profile chosen for the initial temperature appearing in the transition rates.

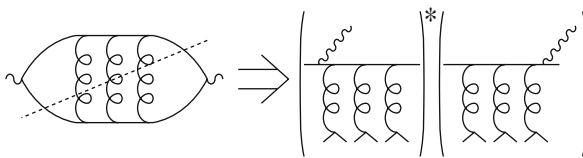


Fig. 11 A typical ladder diagram in the AMY formalism [99]

3.2.5 Models Comparison

The four energy loss formalisms discussed above can be roughly divided into two groups: those calculating the radiated gluon spectrum, i.e. the energy lost by the initial parton (GLV and BDMPS/ASW) and those determining directly the change in the final distribution of the traversing partons (higher twist and AMY). Each approach has its advantages and disadvantages:

- *ASW*: It is applicable to both thin and thick media, but so far lacks an implementation of elastic energy loss.
- *GLV*: It can be applied in confined and deconfined media, but it does not account for the energy flow *into* the medium.
- *Higher twist*: It can directly compute the medium-modified fragmentation functions and allows the study of multi-hadron correlations, but the formalism is more appropriate for thin than thick media.
- *AMY*: It is the only framework that accounts for processes where a thermal gluon or quark can be absorbed by a hard parton, elastic energy loss can be included in a straightforward way, but its application to non-thermalised media is questionable.

All four schemes have independently made successful comparisons to the available data (see Fig. 12 and forthcoming sections). The outcome of the models is one parameter tuned to ideally fit all experimental observables: \hat{q} in the BDMPS/ASW scheme, the initial dN^g/dy density in GLV, the energy loss ε_0 in HT, and the temperature T in AMY. All jet quenching observables in AuAu collisions at 200 GeV can only be reproduced with medium parameters consistent with a QGP at temperatures above the QCD phase transition. The analytical results of the different schemes under “controlled” situations are in principle equivalent, see, e.g., [14]. Yet the detailed comparison of the models is not always straightforward as they

- use different approximations in their calculations,
- do not always include the same list of physics processes (e.g. ΔE_{coll} is neglected in some cases),
- choose a different fitting parameter to characterise the medium, and
- the space–time profile of the quenching medium is not always equivalent.

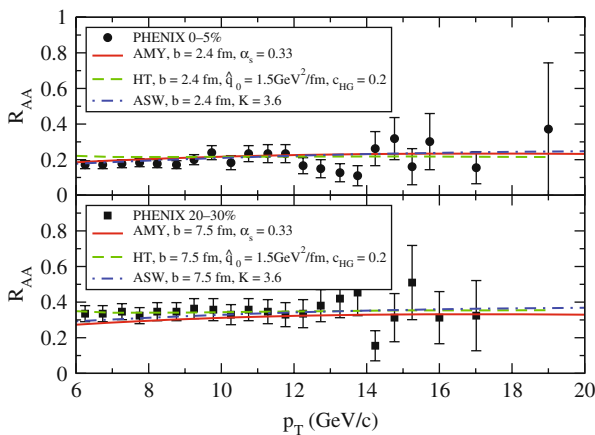


Fig. 12 Suppression factor for high- p_T pions in central (*top*) and semicentral (*bottom*) AuAu collisions at RHIC [100] compared to AMY, HT, and ASW energy loss calculations [101]

The quantitative consistency of the different schemes has been investigated within a 3-dimensional hydrodynamics approach (Fig. 12) [101] linking the various medium properties via thermodynamical relations and using the same space–time evolution. Yet the extracted \hat{q} values still differ by factors of 2–3 (see Sect. 4.2). At least part of the uncertainty is due to the relative insensitivity of the \hat{q} parameter to the irreducible presence of (unquenched) partons emitted from the surface of the plasma [102]. Additional constraints on \hat{q} can be placed by requiring also the reproduction of the suppressed *di-hadron* azimuthal correlations (see Sect. 5.1).

3.3 Jet Quenching Monte Carlos

Ultimately, the discussed energy loss schemes are all based on a final energy rescaling of the vacuum parton-to-hadron fragmentation functions (Fig. 7). Recently, attempts to reformulate parton energy loss as a medium modification of the perturbative *evolution* of the fragmentation functions have been implemented in Monte Carlo (MC) models [56, 103–105]. Such MC approaches allow one to address more detailed experimental observables such as the particle and energy flows within a jet. The DGLAP scale-dependence (Q^2 -evolution) equation of the FFs reads

$$\frac{\partial D_{i \rightarrow h}(x, Q^2)}{\partial \log Q^2} = \sum_j \int_x^1 \frac{dz}{z} \frac{\alpha_s}{2\pi} P_{i \rightarrow j}(z) D_{j \rightarrow h}(x/z, Q^2), \quad (33)$$

with splitting functions $P_{i \rightarrow j}(z)$. The probabilistic nature of parton showering – the “Sudakov factor” $\exp[-\int dQ/Q^2 \int dz \alpha_s/2\pi P_{i \rightarrow j}(z, Q^2)]$ gives the probability that a parton evolves from times t_1 to t_2 without branching – can be easily implemented in MC codes by calculating the virtuality and energy fraction of a parton at each branching point with proper energy-momentum conservation. Parton showers are a basic ingredient of event generators such as PYTHIA [106] or HERWIG [107] which are often used to compare the experimental jet data to the details of the underlying QCD radiation pattern. Medium effects can be easily included by, e.g. modifying the splitting functions in Eq. (33). HYDJET [108, 109] was the first MC code which incorporated medium effects via a PYQUEN routine which modifies the standard PYTHIA branching algorithm to include radiative and elastic energy losses. More recent developments like Q-PYTHIA and Q-HERWIG [40] modify the DGLAP evolution of these two parton-shower MCs. The JEWEL MC [103] implements elastic scattering in DGLAP evolution plus radiative energy loss through a multiplicative constant in the collinear part of the splitting functions [39].

3.4 Parton Energy Loss in AdS/CFT

So far, we have discussed perturbative calculations of parton energy loss in an ideal QGP. Yet the medium produced at RHIC has temperatures $\mathcal{O}(2T_{\text{crit}})$ in a domain

where lattice QCD [2] still predicts large deviations with respect to the asymptotic ideal-gas behaviour. Many experimental signals at RHIC are consistent with the formation of a *strongly coupled* plasma (sQGP) [110–112]. Such a regime is theoretically treatable via the anti-de-Sitter/conformal-field-theory (AdS/CFT) correspondence between weakly coupled gravity and strongly coupled gauge theories [113–115].

The AdS/CFT correspondence conjectures that string theories described in an anti-de-Sitter space¹⁶ times a 5-dimensional sphere ($AdS_5 \times S_5$) are equivalent to a conformal field theory (CFT), defined on the 4-dimensional boundary of this space. A particularly useful case is $\mathcal{N} = 4$ supersymmetric Yang-Mills (SYM)¹⁷ at strong coupling g_{YM} and large number of colours N_c (i.e. at large 't Hooft coupling $\lambda = g_{YM}^2 N_c \gg 1$) which is dual to supergravity in a curved space-time. The string coupling g_s , the curvature radius R of the AdS metric, and the tension $(2\pi\alpha')^{-1}$ of the string are related to the SYM quantities via $R^2/\alpha' = \sqrt{\lambda}$ and $4\pi g_s = g_{YM}^2 = \lambda/N_c$. Essentially, taking the large N_c limit at fixed λ (i.e. weakly coupled gravity: $g_s \rightarrow 0$) and the large λ limit (i.e. weakly curved space and large string tension), the SYM theory can be described by classical gravity in a 5-dimensional space. By virtue of such a duality, one can carry out analytical calculations of gravity, which can then be mapped out “holographically” to the *non-perturbative* dynamics of the gauge sector.

One can further exploit the AdS/CFT correspondence for theories at *finite temperature*, by replacing the AdS_5 space by an AdS Schwarzschild black hole. The temperature of the gauge theory is then equal to the black hole Hawking temperature, $T = r_0/(\pi R^2)$, where r_0 is the coordinate of the black hole horizon. Recent applications of this formalism in the context of heavy-ion physics have led to the determination of transport properties of strongly coupled (SYM) plasmas – such as its viscosity [117], the \hat{q} parameter [118], and the heavy-quark diffusion coefficients [119–122] – from simpler black hole thermodynamics calculations.

In the case of jet quenching calculations [123, 124], one expresses the propagation of a parton through a medium in terms of Wilson lines. The \hat{q} parameter can be identified with the coefficient in the exponential of an adjoint Wilson loop averaged over the medium length: $\langle W^A(C) \rangle \equiv \exp\left[(-1/4\sqrt{2})\hat{q}L^{-2}\right]$ [118]. One then evaluates the gravity dual of this Wilson loop given by the classical action of a string stretching in an $AdS_5 \times S_5$ space with a Schwarzschild black hole background. After solving the equations of motion of the string, the transport coefficient \hat{q} is determined to be

$$\hat{q}_{\text{sym}} = \frac{\pi^{3/2}\Gamma(\frac{3}{4})}{\Gamma(\frac{5}{4})} \sqrt{g^2 N_c} T^3. \quad (34)$$

¹⁶ AdS_5 is a 5-dimensional space with constant and negative curvature.

¹⁷ SYM is a quantum-field $SU(N_c)$ theory like QCD ($\mathcal{N} = 4$ indicates four additional supercharges) but dissimilar from QCD in many aspects: extra SUSY degrees of freedom, no running coupling, no confinement, etc. Yet such differences “wash out” at finite T [116].

Though this result is computed in the infinite coupling and number of colours limits, typical values of $\alpha_s = 0.5$ and $N_c = 3$ lead to $\hat{q} = 4.5 - 20.7 \text{ GeV}^2/\text{fm}$ for $T = 300-500 \text{ MeV}$ [124], consistent with phenomenological fits of the RHIC data [102].

There have also been AdS/CFT-based calculations [119–122] of the diffusion properties of heavy quarks, described by a semiclassical string in the gravity theory, such as the diffusion constant in a $\mathcal{N} = 4$ SYM plasma [120]

$$D \approx \frac{0.9}{2\pi T} \left(\frac{1.5}{\alpha_s N_c} \right)^{1/2}, \quad (35)$$

which agrees with the drag coefficient, see Eq. (3), computed independently.

4 High- p_T Leading Hadron Suppression: Data vs. Theory

The most simple empirically testable (and theoretically computable) consequence of jet quenching is the suppression of the single inclusive high- p_T hadron spectrum relative to that in proton–proton collisions. Since most of the energy of the fragmenting parton goes into a single *leading* hadron, QCD energy loss was predicted to result in a significantly suppressed production of high- p_T hadrons ($R_{AA} \ll 1$) [26, 27]. We compare in this section the existing measurements of large- p_T hadroproduction in pp and AA collisions and discuss their agreement with jet quenching models.

4.1 High- p_T Hadron Spectra in Proton–Proton and Proton–Nucleus Collisions

Figure 13 collects several p_T -differential inclusive cross sections measured at RHIC in pp collisions at $\sqrt{s} = 200 \text{ GeV}$: jets [125], charged hadrons [126], neutral pions [127], direct photons [128], and D , B mesons (indirectly measured via inclusive e^\pm from their semileptonic decays) [129] at central rapidities ($y = 0$) and negative hadrons at forward pseudorapidities ($\eta = 3.2$) [130]. The existing measurements cover nine orders of magnitude in cross section (from 10 mb down to 1 pb) and broad ranges in transverse momentum (from zero for D , B mesons up to 45 GeV/c, a half of the kinematical limit, for jets) and rapidity ($\eta = 0-3.2$).

Standard next-to-leading-order (NLO) [131–138] or resummed next-to-leading log (NLL) [139] pQCD calculations (yellow bands in Fig. 13) with recent proton PDFs [140], fragmentation functions [141, 142], and with varying factorisation-renormalisation scales ($\mu = p_T/2 - 2p_T$) reproduce well the pp data. This is true even in the semi-hard range $p_T \approx 1-4 \text{ GeV}/c$, where a perturbative description would be expected to give a poorer description of the spectra. These results indicate that the hard QCD cross sections at RHIC energies are well under control both experimentally and theoretically in their full kinematic domain.

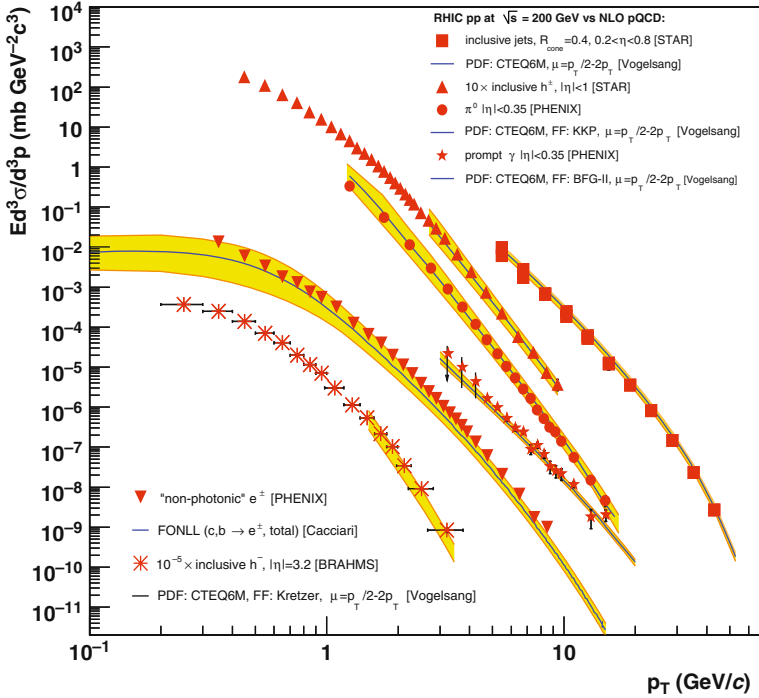


Fig. 13 Compilation of hard cross sections in pp at $\sqrt{s} = 200$ GeV measured by STAR [125, 126], PHENIX [127–129], and BRAHMS [130] (10–30% syst. uncertainties not shown for clarity) compared to NLO [131–138] and NLL [139] pQCD predictions (*yellow bands*)

Not only the proton–proton hard cross sections are well under theoretical control at RHIC but the hard yields measured in deuteron–gold collisions do not show any significant deviation from the perturbative expectations. Figure 14 shows the nuclear modification factors measured in dAu collisions at $\sqrt{s_{NN}} = 200$ GeV for high- p_T π^0 at $y = 0$ [143, 144]. The maximum deviation from the $R_{dAu} = 1$ expectation is of the order of $\sim 10\%$, well accounted for by standard pQCD calculations [145, 146] that include DGLAP-based parametrisations of nuclear shadowing [147] and/or a mild amount of initial-state p_T broadening [148] to account for a modest “Cronin enhancement” [149, 150]. [The only exception to this is baryon (in particular, proton) production which shows a large Cronin enhancement: $R_{dAu} = 1.5\text{--}2.0$ [151].] These data clearly confirm that at RHIC *midrapidities*, the parton flux of the incident gold nucleus can be basically obtained by geometric superposition of the nucleon PDFs and that the nuclear (x , Q^2) modifications of the PDFs are very modest. Since no dense and hot system is expected to be produced in dAu collisions, such results indicate that any deviations from $R_{AA} = 1$ larger than $1 - R_{dAu}^2 \sim 20\%$ potentially observed for hard probes in AuAu collisions (at central rapidities) can only be due to *final-state* effects in the medium produced in the latter reactions.

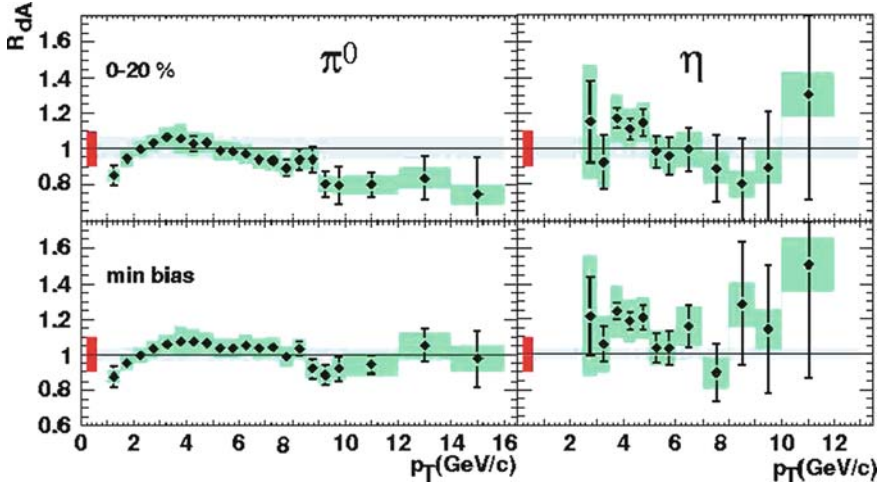


Fig. 14 Nuclear modification factors for high- p_T π^0 (left) and η (right) mesons at midrapidity in d Au collisions at $\sqrt{s_{NN}} = 200$ GeV [143, 144] compared to pQCD calculations [145, 146] with EKS98 [147] nuclear PDFs

4.2 High- p_T Hadron Spectra in Nucleus–Nucleus Collisions

Among the most exciting results from RHIC is the large high- p_T hadron suppression ($R_{AA} \ll 1$) observed in central AuAu compared to pp or d Au reactions. We discuss here the properties of the measured suppression factor and compare it to detailed predictions of parton energy loss models.

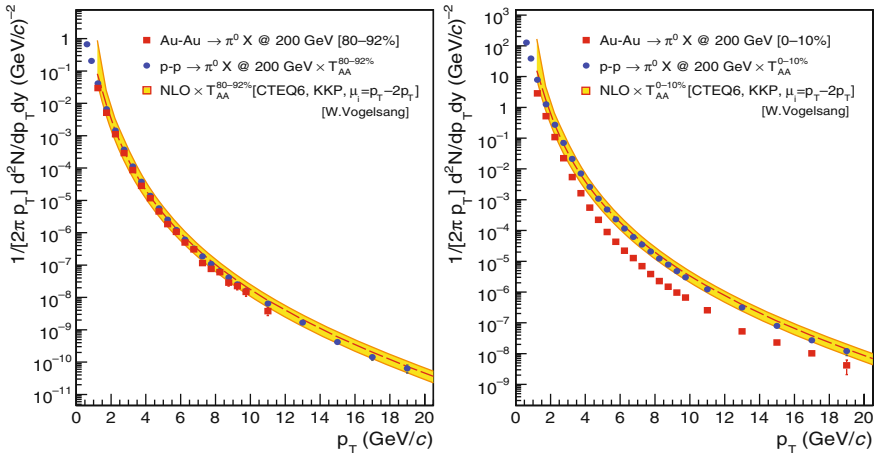


Fig. 15 Invariant π^0 yields measured by PHENIX in peripheral (left) and central (right) AuAu collisions (squares) [100] compared to the (T_{AA} -scaled) pp π^0 cross section (circles) [152] and to a NLO pQCD calculation (curves and yellow band) [131–133]

(a) *Magnitude of the suppression: medium properties*

Figure 15 shows the π^0 spectrum measured in pp collisions [152] compared to peripheral (*left*) and central (*right*) AuAu spectra [100] at 200 GeV, as well as to NLO pQCD calculations [131–133]. Whereas the peripheral AuAu spectrum is consistent with a simple superposition of individual NN collisions, the data in central AuAu show a suppression factor of 4–5 with respect to this expectation.

The amount of suppression is better quantified taking the ratio of both spectra in the nuclear modification factor, Eq. (23). Figure 16 compiles the measured $R_{AA}(p_T)$ for various hadron species and for direct γ in central AuAu collisions at $\sqrt{s_{NN}} = 200$ GeV. Above $p_T \approx 5$ GeV/c, π^0 [153], η [154], and charged hadrons [126, 155] (dominated by π^\pm [155]) all show a common factor of ~ 5 suppression relative to the $R_{AA} = 1$ expectation that holds for hard probes, such as direct photons, which do not interact with the medium [156]. The fact that $R_{AA} \approx 0.2$ irrespective of the nature of the finally produced hadron is consistent with a scenario where final-state energy loss of the *parent* parton takes place *prior* to its fragmentation into hadrons in the vacuum according to *universal* (but energy-rescaled) FFs. The suppression factor at top RHIC energies is very close to the “participant scaling”, $(N_{\text{part}}/2)/N_{\text{coll}} \approx 0.17$, expected in the strong quenching limit where only hadrons produced at the *surface* of the medium reach the detector without modifications [157]. From the R_{AA} one can approximately obtain the fraction of energy lost, $\varepsilon_{\text{loss}} = \Delta p_T/p_T$, via

$$\varepsilon_{\text{loss}} \approx 1 - R_{AA}^{1/(n-2)}, \quad (36)$$

when both the AuAu and pp -invariant spectra are power laws with exponent n , i.e. $1/p_T dN/dp_T \propto p_T^{-n}$ [158].

The high- p_T AuAu suppression can be well reproduced by parton energy loss models that assume the formation of a very dense system with initial gluon rapidity densities $dN^g/dy \approx 1400$ (yellow line in Fig. 16) [160, 161], transport coefficients $\langle \hat{q} \rangle \approx 13$ GeV²/fm (red line in Fig. 17, left) [89], or plasma temperatures $T \approx 400$ MeV [83]. The quality of agreement between the theory and data has been studied in detail in [162, 100] taking into account the experimental (though not theoretical) uncertainties. The PHENIX π^0 suppression constrains the PQM model [89] transport coefficient $\langle \hat{q} \rangle$ as $13.2^{+2.1}_{-3.2}$ and $^{+6.3}_{-5.2}$ GeV²/fm at the one and two standard deviation levels (Fig. 17).

The consistency between the extracted \hat{q} , dN^g/dy , and T values in the various models can be cross-checked considering the simple case of a gluon traversing a thermalised gluon plasma. The transport coefficient, Eq. (2), is the product of the particle density, the medium Debye mass, and the parton-medium cross section. Taking $\sigma_{gg} = 9\pi\alpha_s^2/(2m_D^2)$ with $\alpha_s = 0.5$ for the latter, one has a simple relation¹⁸ between \hat{q} and ρ :

¹⁸ Conversion between units is done multiplying by suitable powers of $\hbar c = 0.197$ GeV fm.

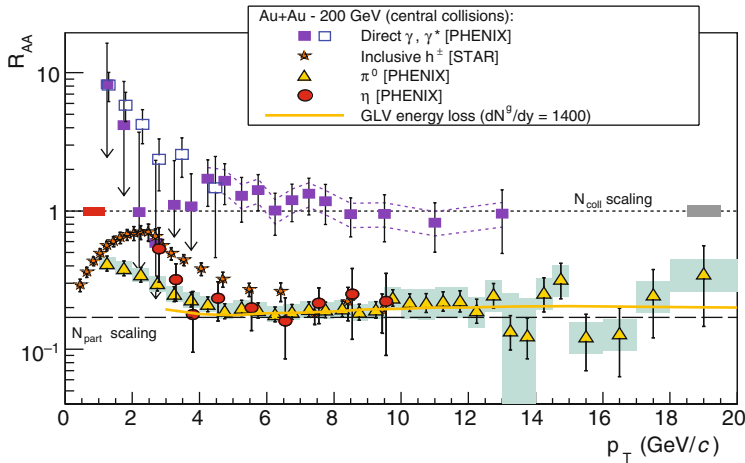


Fig. 16 $R_{AA}(p_T)$ measured in central AuAu at 200 GeV for π^0 [100] and η [154] mesons, charged hadrons [126], and direct photons [156, 159] compared to theoretical predictions for parton energy loss in a dense medium with $dN^g/dy = 1400$ (yellow curve) [160, 161]

$$\hat{q}[\text{GeV}^2/\text{fm}] = m_D^2 \times \sigma \times \rho = m_D^2 \times 9\pi\alpha_s^2/(2m_D^2) \times \rho \approx 0.14 K \rho[\text{fm}^{-3}], \quad (37)$$

where we introduce the K factor to account for possible higher order scatterings not included in the LO perturbative cross section. For an ideal ultrarelativistic gas, the particle density scales with the cube of the temperature as $\rho \approx \text{ndf}/9 \cdot T^3$. For a pure gluon plasma, with $\text{ndf} = 16$, $\rho[\text{fm}^{-3}] \approx 260 \cdot (T[\text{GeV}])^3$, and one can write Eq. (37) as

$$\hat{q}[\text{GeV}^2/\text{fm}] \approx 36 K \cdot (T[\text{GeV}])^3. \quad (38)$$

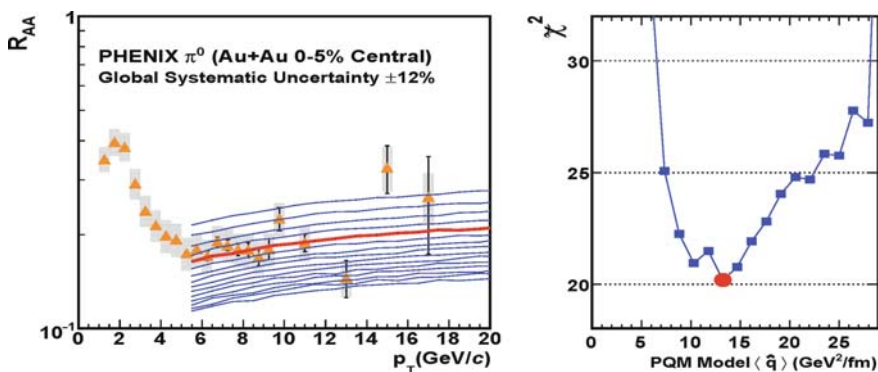


Fig. 17 *Left*: $R_{AA}(p_T)$ for neutral pions in central AuAu collisions [100] compared to PQM model calculations [89] for varying values of the \hat{q} coefficient (red curve, best fit). *Right*: Corresponding (data vs. theory) χ^2 values for the fitted PQM \hat{q} parameter [162]

In addition, as particle and energy densities are related by $\rho[\text{fm}^{-3}] \approx 1.9 \cdot (\varepsilon[\text{GeV}/\text{fm}^3])^{3/4}$, one can express Eq. (37) also as $\hat{q}[\text{GeV}^2/\text{fm}] \approx 0.27 K \cdot (\varepsilon[\text{GeV}/\text{fm}^3])^{3/4}$. In an expanding plasma, the density follows a power law evolution as a function of time, $\rho = \rho_0 (\tau_0/\tau)^\alpha$, and thus so does the transport coefficient (37):

$$\hat{q}(\tau)[\text{GeV}^2/\text{fm}] \approx 0.14 K \cdot \rho_0 \left(\frac{\tau_0}{\tau}\right)^\alpha = 0.14 K \cdot \frac{dN^g}{dV} \left(\frac{\tau_0}{\tau}\right) \approx 0.14 K \cdot \frac{1}{A_T} \frac{dN^g}{dy} \frac{1}{\tau}, \quad (39)$$

where for the two last equalities we have assumed a 1-dimensional (aka Bjorken) longitudinal expansion, i.e. $\alpha = 1$ and $dV = A_T \tau_0 dy$, where $A_T[\text{fm}^2]$ is the transverse area of the system. Combining Eq. (39) with Eq. (27) that relates the *time-averaged* $\hat{q}(\tau)$ to that of a static medium with effective length L_{eff} , we finally get

$$\langle \hat{q} \rangle [\text{GeV}^2/\text{fm}] \approx 0.14 K \cdot \frac{2}{L_{\text{eff}}[\text{fm}] A_T[\text{fm}^2]} \frac{dN^g}{dy} \approx 1.4 \cdot 10^{-3} \cdot K \cdot \frac{dN^g}{dy}, \quad (40)$$

where, for the last equality, we use $L_{\text{eff}} \approx 2 \text{ fm}$ and $\langle A_T \rangle \approx 100 \text{ fm}^2$ for the overlap area in 0–10% most central AuAu. This approximate relation between the average transport coefficient and the original gluon density is only well fulfilled by the data (see Table 2 below) for a very large $K \approx 7$ factor. The fact that the jet quenching data favour an effective elastic parton-medium cross section much larger than the LO perturbative estimate ($\sigma_{gg} \approx 1.5 \text{ mb}$) has been discussed many times in the literature – e.g. in the context of the strong partonic elliptic flow seen in the data [163, 164] – and supports the strongly coupled nature of the QGP produced at RHIC.

A more detailed comparison of different energy loss schemes within a realistic 3-dimensional hydrodynamics evolution has been carried out in [165]. The extraction of a common \hat{q} parameter from the different model predictions relies on additional assumptions about the (thermo)dynamical state of the produced matter. The results for ASW, AMY, and HT are shown in Table 1 (last two rows). The ASW calculations consistently predict a higher \hat{q}_0 than AMY or HT. These differences can be traced to uncertainties of the thermodynamical scaling choice ($\hat{q} \propto T^3$ or $\varepsilon^{3/4}$) and to the initial time where the medium is supposed to start to quench (hydro

Table 1 Medium parameters derived in various parton energy loss schemes that reproduce the high- p_T π^0 suppression in central AuAu [100]. The last two rows are from a 3-dimensional hydro simulation with two choices of $\hat{q}(\mathbf{r}, \tau)$ scaling with the local thermal properties of the plasma (T_0, ε_0) [165]

Medium parameter	ASW	HT	AMY
$\langle \hat{q} \rangle$	13 GeV ² /fm (PQM)	–	–
T_0	–	–	0.4 GeV
$\hat{q}_0 \propto \varepsilon_0^{3/4}(\mathbf{r}, \tau)$	18.5 GeV ² /fm	4.5 GeV ² /fm	–
$\hat{q}_0 \propto T_0^3(\mathbf{r}, \tau)$	10 GeV ² /fm	2.3 GeV ² /fm	4.1 GeV ² /fm

calculations at RHIC often start at $\tau_0 = 0.6$ fm/c). In addition, AMY accounts for collisional losses which are neglected in the purely radiative ASW approach.

(b) *Centre-of-mass energy dependence*

As one increases the centre-of-mass energy in nucleus–nucleus collisions, the produced plasma reaches higher energy and particle densities and the system stays longer in the QGP phase. Since $\Delta E_{\text{loss}} \propto dN^g/dy \propto dN_{ch}/d\eta$, and since the charged particle multiplicity in AA at midrapidity increases with collision energy as [166, 167]

$$dN_{ch}/d\eta \approx 0.75 \cdot (N_{part}/2) \cdot \ln(\sqrt{s_{NN}} [\text{GeV}]/1.5), \quad (41)$$

one naturally expects the hadron quenching to increase accordingly with $\sqrt{s_{NN}}$. The actual “excitation function” of the suppression factor is only approximately given by Eq. (41) because for increasing energies other factors play competing roles: (i) the lifetime of the quenching medium becomes longer, (ii) the parton spectrum becomes flatter leading to a comparatively smaller suppression for the same value of ΔE_{loss} (see next), and (iii) the fraction of quarks and gluons produced at a fixed p_T changes (see Fig. 22 below and the associated colour factor discussion).

Figure 18 compiles the measured $R_{AA}(p_T)$ for high- p_T π^0 in central AA collisions in the range $\sqrt{s_{NN}} \approx 20 - 200$ GeV compared to parton energy loss calculations that assume the formation of systems with initial gluon densities per unit rapidity in the range $dN^g/dy \approx 400 - 1400$ [160, 161, 171] or, equivalently, averaged transport coefficients $\langle \hat{q} \rangle \approx 3.5 - 13$ GeV²/fm [74] (Table 2). As can be seen from Eq. (36), R_{AA} depends not only on ΔE_{loss} but also on the steepness (power law exponent n) of the parton p_T spectrum. With decreasing $\sqrt{s_{NN}}$, the p_T spectra become steeper effectively leading to a larger suppression (i.e. smaller R_{AA}) for the

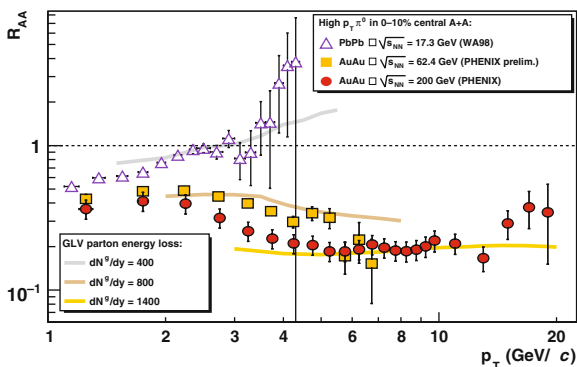


Fig. 18 Nuclear modification factor, $R_{AA}(p_T)$, for neutral pions in central PbPb at $\sqrt{s_{NN}} = 17.3$ GeV [168, 169] and AuAu at $\sqrt{s_{NN}} = 62.4$ GeV [170], 200 GeV [153]; compared to GLV energy loss calculations for initial gluon densities: $dN^g/dy = 400, 800, 1400$ [160, 161, 171], respectively. Experimental normalisation errors, $\mathcal{O}(10-25\%)$, not shown

same ΔE_{loss} . The SPS data show an R_{AA} for central PbPb which, though consistent with unity [169], is significantly suppressed compared to the ‘‘Cronin enhancement’’ observed for peripheral PbPb and for pPb collisions [172].

For each collision energy, the derived values for dN^s/dy are consistent with the final charged hadron density $dN_{\text{ch}}/d\eta$ measured in the reactions. Indeed, assuming an isentropic¹⁹ expansion process, all the hadrons produced at midrapidity in a AA collision come directly from the original gluons released²⁰:

$$\frac{dN^s}{dy} \approx \frac{N_{\text{tot}}}{N_{\text{ch}}} \left| \frac{d\eta}{dy} \right| \frac{dN_{\text{ch}}}{d\eta} \approx 1.8 \cdot \frac{dN_{\text{ch}}}{d\eta}. \quad (42)$$

This relation is relatively well fulfilled by the data as can be seen by comparing the fourth and fifth columns of Table 2.

Table 2 Initial gluon densities dN^s/dy [160, 161, 171], and transport coefficients $\langle \hat{q} \rangle$ [89] for the dense media produced in central AA collisions at SPS and RHIC energies obtained from parton energy loss calculations reproducing the observed high- p_T π^0 suppression at each $\sqrt{s_{NN}}$. The measured charged particle densities at midrapidity, $dN_{\text{ch}}^{\text{exp}}/d\eta$ [166, 167], are also quoted

	$\sqrt{s_{NN}}$ (GeV)	$\langle \hat{q} \rangle$ (GeV ² /fm)	dN^s/dy	$dN_{\text{ch}}^{\text{exp}}/d\eta$
SPS	17.3	3.5	400	312 ± 21
RHIC	62.4	7.	800	475 ± 33
RHIC	130.	~11	~1000	602 ± 28
RHIC	200.	13	1400	687 ± 37

(c) p_T -dependence of the suppression

At RHIC top energies, the quenching factor remains constant from 5 GeV/c up to the highest transverse momenta measured so far, $p_T \approx 20$ GeV/c (Fig. 16). The flatness of $R_{AA}(p_T)$ was not expected since many original analytical calculations based on the LPM effect (see, e.g., [173]) predicted an R_{AA} slowly (logarithmically) increasing with p_T . However, the combined effect of (i) kinematics constraints (which modify the asymptotic ΔE_{loss} formulas), (ii) the steeply falling p_T spectrum of the scattered partons, and (iii) $\mathcal{O}(20\%)$ p_T -dependent (anti)shadowing differences between the proton and nuclear PDFs included in the various models [160, 161, 171, 82, 102] results in an effectively flat $R_{AA}(p_T)$ as found in the data.

The much larger kinematical range opened at LHC energies will allow to test the p_T -dependence of parton energy loss over a much wider domain than at RHIC. The GLV and PQM predictions for the charged hadron suppression in PbPb at 5.5 TeV are shown in Fig. 19. Apart from differences in the absolute quenching factor, PQM

¹⁹ Namely, expanding at constant entropy, i.e. without extra particle production.

²⁰ We use $N_{\text{tot}}/N_{\text{ch}} = 3/2$ and the Jacobian $|d\eta/dy| = E/m_T \approx 1.2$ for a mostly pionic system.

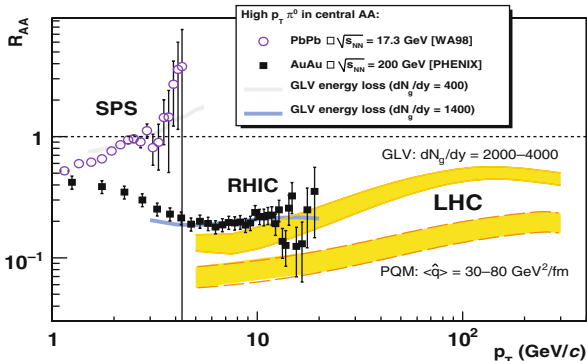


Fig. 19 $R_{AA}(p_T)$ for neutral pions at SPS [168, 169] and RHIC [100] compared to the expected suppression of charged hadrons in central PbPb at the LHC ($\sqrt{s_{NN}} = 5.5$ TeV) by the GLV ($dN^s/dy = 2000-4000$) [160, 161] and PQM ($\langle \hat{q} \rangle \approx 30-80 \text{ GeV}^2/\text{fm}$) [89, 90] models

seemingly predicts a slower rise of $R_{AA}(p_T)$ than GLV. The large p_T reaches of the ALICE [174], ATLAS [175], and CMS [176] experiments (up to 300 GeV/c for the nominal luminosities) will allow them to test such level of model details.

(d) Centrality (system-size) dependence

The volume of the overlap zone in a heavy-ion collision can be “dialed” either by selecting a given impact parameter b – i.e. by choosing more central or peripheral reactions – or by colliding larger or smaller nuclei. From Eq. (14), the relative amount of suppression depends²¹ on the effective mass number A_{eff} or, equivalently, on the number of participant nucleons N_{part} as $\varepsilon = \Delta E/E \propto A_{\text{eff}}^{2/3} \propto N_{\text{part}}^{2/3}$. Combining this expression with Eq. (36) yields [177]

$$R_{AA} = \left(1 - \kappa N_{\text{part}}^\alpha\right)^{n-2},$$

with $\alpha \approx 2/3$ and κ an arbitrary constant. (43)

Figure 20 (*left*) compares the measured high- p_T pion suppression in CuCu and AuAu at $\sqrt{s_{NN}} = 200$ GeV [178, 179]. Because of the large difference in the Cu ($A = 63$) and Au ($A = 197$) atomic masses, the same N_{part} value (same overlap volume) implies very different collision geometries: a thin, elongated collision zone in AuAu and a thicker, more spherical one in the CuCu case. Yet interestingly the average suppression in the two systems depends only on N_{part} . Fitting this dependence with expression (43) yields $\alpha = 0.56 \pm 0.10$, consistent with $\alpha \approx 0.6$ expected in parton energy loss scenarios [100, 177].

²¹ Since $dN^s/dy \propto dN_{\text{ch}}/dy \propto A_{\text{eff}} \propto N_{\text{part}}$, $L \propto A_{\text{eff}}^{1/3} \propto N_{\text{part}}^{1/3}$, and $A_{\perp} \propto A_{\text{eff}}^{2/3} \propto N_{\text{part}}^{2/3}$.

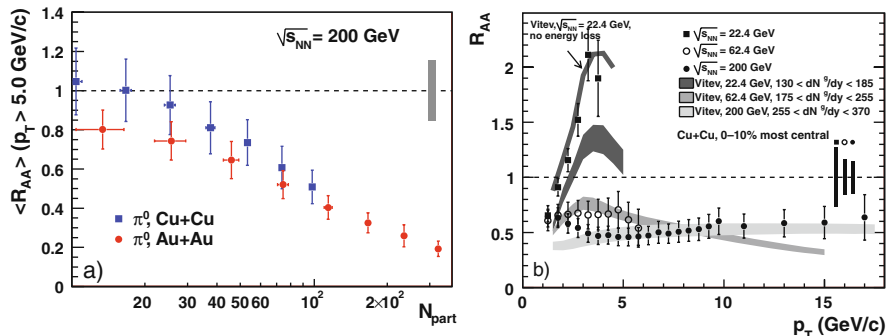


Fig. 20 *Left*: Centrality (N_{part}) dependence of the high- p_T π^0 suppression in CuCu and AuAu at 200 GeV [179]. *Right*: $R_{AA}(p_T)$ for π^0 in central CuCu collisions at 22.4, 62.4, and 200 GeV compared to GLV calculations with initial gluon densities $dN^g/dy \approx 100\text{--}370$ [178]

Figure 20 (*right*) shows the $R_{AA}(p_T)$ measured in CuCu at 22.4, 62.4, and 200 GeV. The amount of suppression observed is roughly a factor $(A_{Au}/A_{Cu})^{2/3} \approx 2$ lower than in AuAu at the same energies (Fig. 18). The $R_{AA}(p_T)$ can be described by GLV with initial gluon densities $dN^g/dy \approx 100\text{--}370$ (the CuCu enhancement at 22.4 GeV is actually consistent with a scenario *without* parton energy loss).

(e) Path-length dependence

The *quadratic* dependence of the energy loss on the thickness of the medium L , Eq. (11), becomes a *linear* dependence on the *initial* value of L when one takes into account the expansion of the plasma. Experimentally, one can test the L -dependence of parton suppression by exploiting the spatial asymmetry of the system produced in non-central nuclear collisions (Fig. 21, *left*). Partons produced “in plane” (“out of

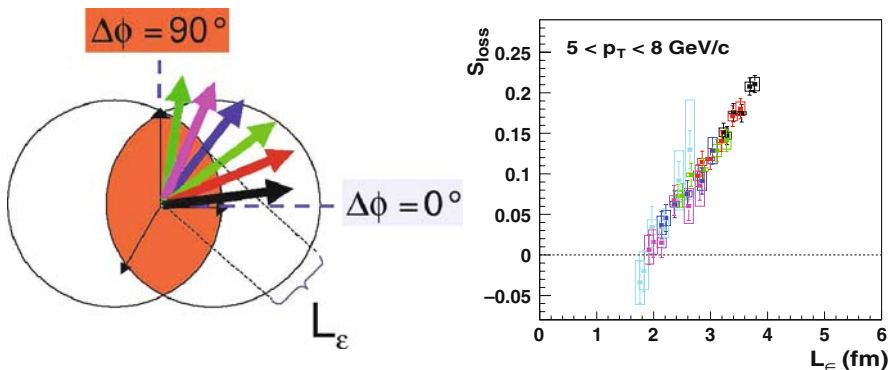


Fig. 21 *Left*: Effective thicknesses along various azimuthal directions with respect to the reaction plane in the overlap region of two heavy ions. *Right*: Fraction of energy loss S_{loss} vs. effective path-length L_ϵ measured for high- p_T neutral pions in AuAu at 200 GeV [158]

plane”), i.e. along the short (long) direction of the ellipsoid matter with eccentricity ε will comparatively traverse a shorter (longer) thickness.

PHENIX [158] has measured the high- p_T neutral pion suppression as a function of the angle with respect to the reaction plane, $R_{AA}(p_T, \phi)$. Each azimuthal angle ϕ can be associated with an average medium path-length L_ε via a Glauber model. Figure 21 (*right*) shows the measured fractional energy loss $S_{\text{loss}}(\phi)$, obtained via Eq. (36), as a function of L_ε for pions in the range $p_T = 5\text{--}8$ GeV/c (markers of different colours correspond to varying centralities, i.e. eccentricities ε). The energy loss is found to satisfy the expected $\Delta E_{\text{loss}} \propto L$ dependence above a minimum length of $L \approx 2$ fm. The absence of suppression in the surface of the medium is explained as due to a geometric “corona” effect [180].

(f) Non-Abelian (colour factor) dependence

The amount of energy lost by a parton in a medium is proportional to its colour Casimir factor C_R (i.e. $C_A = 3$ for gluons, $C_F = 4/3$ for quarks). Asymptotically, the probability for a gluon to radiate another gluon is $C_A/C_F = 9/4$ times larger than for a quark and, thus, g -jets are expected to be more quenched than q -jets in a QGP. One can test such a genuine *non-Abelian* property of QCD energy loss in two ways:

- (1) by measuring hadron suppression at a *fixed* p_T for *increasing* \sqrt{s} [181, 182],
- (2) by comparing the suppression of high- p_T (*anti*)*protons* (coming mostly from gluon fragmentation) to that of *pions* (which come from both g and q, \bar{q}).

The motivation for (1) is based on the fact that the fraction of quarks and gluons scattered at midrapidity in a pp or AA collision at a *fixed* p_T varies with $\sqrt{s_{NN}}$ in a proportion given²² by the relative density of q, \bar{q} , and g at the corresponding Bjorken $x = 2p_T/\sqrt{s}$ in the proton/nucleus. At large (small) x , hadroproduction is dominated by quark (gluon) scatterings. A full NLO calculation [131–133] (Fig. 22, *left*) predicts that hadrons with $p_T \approx 5$ GeV/c at SPS (LHC) energies are $\sim 100\%$ produced by valence quarks (gluons), whereas at RHIC they come 50–50% from both species.

Figure 22 (*right*) shows the R_{AA} for 4-GeV/c pions measured at SPS and RHIC compared to two parton energy loss curves, both normalised at the $R_{AA} \approx 1$ measured at SPS and extrapolated all the way up to LHC energies [182]. The lower curve shows the expected R_{AA} assuming the normal non-Abelian behaviour ($\Delta E_g/\Delta E_q = 9/4$). The upper (dotted) curve shows an arbitrary prescription in which quarks and gluons lose the same energy ($\Delta E_g = \Delta E_q$). Above $\sqrt{s_{NN}} \approx 100$ GeV, gluons take over as the dominant parent parton of hadrons with $p_T \approx 5$ GeV/c and, consequently, the R_{AA} values drop faster in the canonical non-Abelian scenario.

²² The different “hardness” of quarks and gluons fragmenting into a given hadron at the corresponding $z = p_{\text{hadron}}/p_{\text{parton}}$ plays also a (smaller) role.

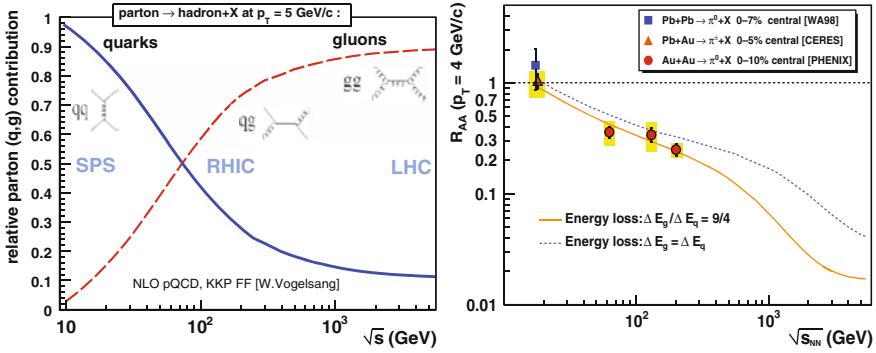


Fig. 22 *Left*: Relative fraction of quarks and gluons fragmenting into a hadron at $p_T = 5 \text{ GeV}/c$ in pp collisions in the range $\sqrt{s} = 10\text{--}5500 \text{ GeV}$ given by NLO pQCD [131–133]. *Right*: $R_{AA}(p_T = 4 \text{ GeV}/c)$ for π^0 in central AA collisions as a function of collision energy compared to non-Abelian (solid) and “non-QCD” (dotted) energy loss curves [181, 182]

The experimental high- $p_T \pi^0$ data supports the expected colour factor dependence of $R_{AA}(\sqrt{s_{NN}})$ [181].

The second test of the colour charge dependence of hadron suppression is based on the fact that gluons fragment comparatively more into (anti)protons than quarks do. One would thus naively expect $R_{AA}^{p,\bar{p}} < R_{AA}^{\pi}$. The STAR results (Fig. 23, left) are, however, seemingly at variance with this expectation: pions appear more suppressed than protons at high- p_T [183]. The use of (anti)protons as a perturbative reference for particle production is, however, questionable: p, \bar{p} are already found to be enhanced in dAu compared to pp collisions by a factor $\sim 50\text{--}100\%$ for p_T ’s as large as $7 \text{ GeV}/c$ [151]. It is likely that there is an extra mechanism of baryon production, based, e.g. on in-medium quark coalescence [185–187], which compensates for the energy loss suffered by the parent partons. It is also important to

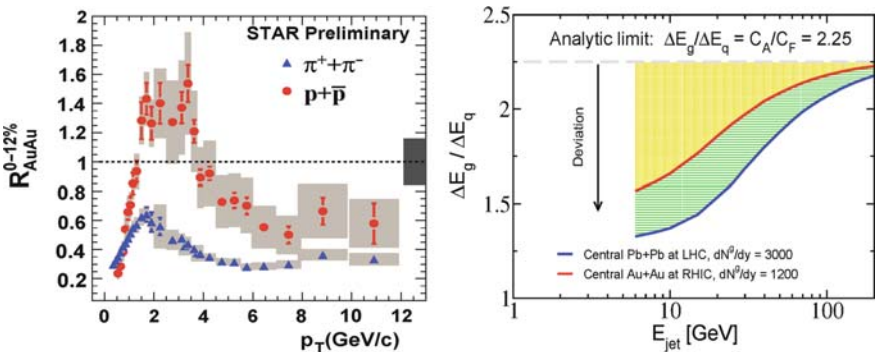


Fig. 23 *Left*: $R_{AA}(p_T)$ for pions and (anti)protons in central AuAu at $\sqrt{s_{NN}} = 200 \text{ GeV}$ [183]. *Right*: Comparison between ΔE_g and ΔE_q in central collisions of large nuclei at RHIC and LHC showing large deviations from $\Delta E_g = 2.25\Delta E_q$ for finite parton energies [184]

stress that the $\Delta E_g/\Delta E_q = 9/4$ expectation holds only for asymptotic parton energies. Finite energy constraints yield values $\Delta E_g/\Delta E_q \approx 1.5$ for realistic kinematics (Fig. 23, right) [184].

(g) *Heavy-quark mass dependence*

A robust prediction of QCD energy loss models is the hierarchy $\Delta E_Q < \Delta E_q < \Delta E_g$. Due to the dead cone effect, the radiative energy loss for a charm (bottom) quark is $\sim 25\%$ (75%) less than for a light quark (see Sect. 2.2). Surprisingly, PHENIX and STAR measurements of high- p_T electrons from the semileptonic decays of D and B mesons indicate that their suppression is comparable to that of light mesons, $R_{AA}(Q) \sim R_{AA}(q, g) \approx 0.2$ (Fig. 24, left) [188–190]. Such a low R_{AA} cannot be described by radiative energy loss calculations with the same initial gluon densities or transport coefficients needed to quench the light hadron spectra [191, 192].

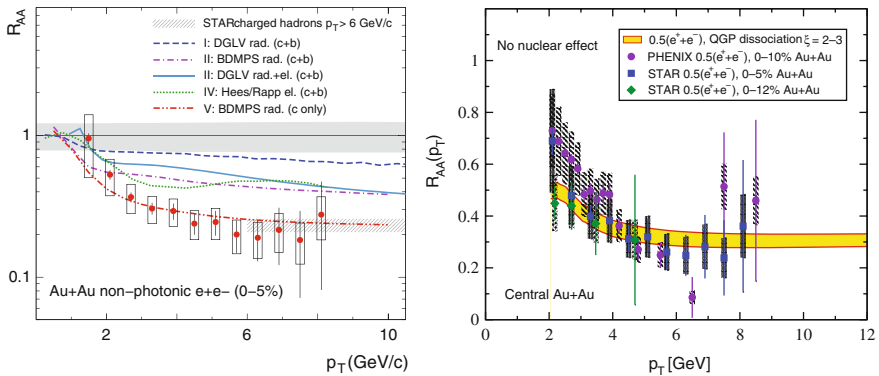


Fig. 24 $R_{AA}(p_T)$ for decay electrons from D and B mesons in central AuAu at $\sqrt{s_{NN}} = 200$ GeV [188–190] compared to various radiative+elastic energy loss models for c and b quarks (*left*) and to a model of D and B meson dissociation in the plasma [196] (*right*)

Various explanations have been proposed to solve the “heavy flavour puzzle”:

- First, if only c quarks (three times more suppressed than the heavier b quarks) actually contributed to the measured high- p_T decay electron spectrum, then one would indeed expect $R_{AA}(c) \approx 0.2$ [192]. Yet indirect measurements from PHENIX [193] and STAR [194] have confirmed the similar production yields of electrons from D and B mesons above $p_T \approx 5$ GeV/ c predicted by NLL pQCD [195].
- The heavy-quark suppression has revived the interest of computing *elastic* energy loss in a QGP [197, 21, 198, 22]. As discussed in Sect. 2.2, ΔE_{el} can indeed be a significant contribution for heavy quarks (see “rad+el” curves in Fig. 24, *left*).
- The strongly coupled nature of the plasma at RHIC would lead, according to AdS/CFT calculations [119–122, 199], to a larger heavy-quark momentum dif-

fusion parameter than expected in perturbative approaches [200]. This would explain the larger charm/bottom quenching observed in the data.

- Two works [201, 202] argue that the large charm-quark coalescence into Λ_c baryons (with a small semileptonic decay branching ratio) in the plasma would deplete the number of open-charm mesons and correspondingly reduce the number of decay electrons compared to pp collisions.
- The assumption of vacuum hadronisation (after in-medium radiation) implicit in all parton energy loss formalisms may well not hold in the case of a heavy quark. All existing quark-hadronisation time estimates [148] are inversely proportional to the mass m_h of the final produced hadron. The heavier the hadron, the faster the formation. In the rest frame²³ of the fragmenting heavy-Q the formation time of D and B mesons [196]

$$\tau_{\text{form}} = \frac{1}{1 + \beta_Q} \frac{2z(1-z)p^+}{\mathbf{k}^2 + (1-z)m_h^2 - z(1-z)m_Q^2},$$

where $\beta_Q = p_Q/E_Q$, (44)

is of order $\tau_{\text{form}} \approx 0.4\text{--}1$ fm/c, respectively. Thus, theoretically, one needs to account for the energy loss of the heavy quark in the medium as well as for the dissociation rate of the heavy-quark *meson* inside the QGP. The expected amount of suppression in that case is larger and consistent with the data (Fig. 24, *right*).

5 High- p_T Di-hadron ϕ , η Correlations: Data vs. Theory

Beyond the leading hadron spectra discussed in the previous section, detailed studies of the modifications of the jet structure in heavy-ion collisions have been addressed via high- p_T multi-particle (mostly di-hadron) ϕ , η correlations. Jet-like correlations are measured on a *statistical* basis by selecting high- p_T *trigger* particles and measuring the azimuthal ($\Delta\phi = \phi - \phi_{\text{trig}}$) and pseudorapidity ($\Delta\eta = \eta - \eta_{\text{trig}}$) distributions of *associated* hadrons ($p_T^{\text{assoc}} < p_T^{\text{trig}}$) relative to the trigger:

$$C(\Delta\phi, \Delta\eta) = \frac{1}{N_{\text{trig}}} \frac{d^2 N_{\text{pair}}}{d\Delta\phi d\Delta\eta}. \quad (45)$$

Combinatorial background contributions, corrections for finite pair acceptance, and the superimposed effects of *collective* azimuthal modulations (elliptic flow) can be taken care of with different techniques [203–205]. A commonly used $C(\Delta\phi)$ background-subtraction method is the “zero yield at minimum” (ZYAM) [206].

A schematic representation of the di-hadron azimuthal-pseudorapidity correlations $dN_{\text{pair}}/d\Delta\phi d\eta$ measured in pp and central AuAu collisions is shown in Fig. 25. In the pp case, without significant initial- or final-state interactions, a dijet signal appears clearly as two distinct back-to-back Gaussian-like peaks at $\Delta\phi \approx 0$,

²³ Note that in the lab system there is an extra Lorentz boost factor: $\tau_{\text{lab}} = \gamma_Q \cdot \tau_{\text{form}}$.

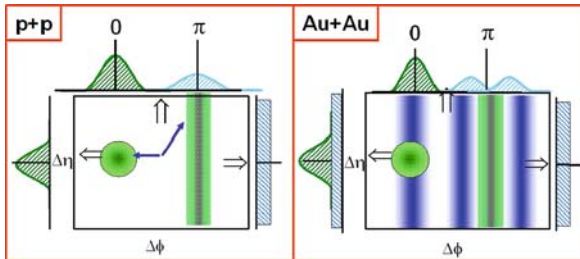


Fig. 25 Schematic illustration summarising the jet-induced di-hadron correlation signals in $\Delta\phi$ and $\Delta\eta$ observed in pp (left) and central AuAu (right) at $\sqrt{s_{NN}} = 200$ GeV [207]

$\Delta\eta \approx 0$ (near-side), and $\Delta\phi \approx \pi$ (away-side). The away-side peak is broader in $\Delta\eta$ (up to $\Delta\eta \approx 2$) than the near-side peak due to the *longitudinal* momentum imbalance between the two colliding partons with different x_1, x_2 momentum fractions (the collision is boosted in η in the direction of the larger $x_{1,2}$). At variance with such a standard dijet topology, the di-hadron correlations in AuAu reactions at RHIC show several striking features, discussed in detail below:

- The *away-side* azimuthal peak at $\Delta\phi \approx \pi$ *disappears* with increasing centrality for hadrons with $p_T^{\text{assoc}} \lesssim 5$ GeV/c, consistent with strong suppression of the leading fragments of the recoiling jet traversing the medium [203].
- The vanishing of the away-side peak is accompanied with an *enhanced* production of *lower* p_T hadrons ($p_T^{\text{assoc}} \lesssim 2.5$ GeV/c) [205, 204] with a characteristic *double-peak* structure at $\Delta\phi \approx \pi \pm 1.1$ –1.3.
- One observes a large *broadening* (“ridge”), out to $\Delta\eta \approx 4$, of the *near-side pseudorapidity* $dN_{\text{pair}}/d\Delta\eta$ correlations [204].

5.1 Azimuthal Correlations: Away-Side Quenching and Energy Loss

Figure 26 shows the increasingly distorted back-to-back azimuthal correlations in high- p_T triggered central AuAu events as one decreases the p_T of the associated hadrons (right to left). Whereas compared to pp the near-side peak remains unchanged for all p_T 's, the away-side peak is only present for the highest partner p_T 's but progressively disappears for less energetic partners [208, 209]. Early STAR results [203] showed a monojet-like topology with a complete disappearance of the opposite-side peak for $p_T^{\text{assoc}} \approx 2 - 4$ GeV/c.

For any range of trigger p_T^{trig} and associated p_T^{assoc} intervals, the correlation strength over an azimuthal range $\Delta\phi$ between a trigger hadron h_t and a partner hadron h_a in the opposite azimuthal direction can be constructed as a function of the momentum fraction $z_T = p_T^{\text{assoc}}/p_T^{\text{trig}}$ via a “pseudo-fragmentation function” [210]:

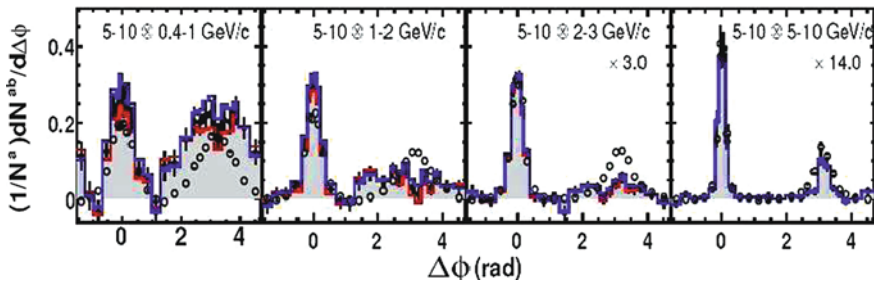


Fig. 26 Comparison of the azimuthal di-hadron correlation $dN_{\text{pair}}/d\Delta\phi d\eta$ for pp (open symbols) and central AuAu (closed symbols) at $\sqrt{s_{NN}} = 200$ GeV for $p_T^{\text{trig}} = 5\text{--}10$ GeV/c and increasingly smaller (right to left) values of p_T^{assoc} [209]

$$D_{pp(AA)}^{\text{away}}(z_T) = \int_{p_T^{\text{trig, min}}^{\text{trig}}}^{p_T^{\text{trig, max}}} dp_T^{\text{trig}} \int_{p_T^{\text{assoc, min}}^{\text{assoc}}}^{p_T^{\text{assoc, max}}} dp_T^{\text{assoc}} \int_{\text{away}} d\Delta\phi \frac{d^3\sigma_{pp(AA)}^{h_i, h_a}/dp_T^{\text{trig}} dp_T^{\text{assoc}} d\Delta\phi}{d\sigma_{pp(AA)}^{h_i}/dp_T^{\text{trig}}} \quad (46)$$

Figure 27 (left) shows the measured D_{AA}^{away} distributions for pp and AuAu collisions as a function of z_T compared to predictions of the HT parton energy loss model [211] for various values of the ε_0 parameter quantifying the amount of energy loss. Similarly to $R_{AA}(p_T)$, the magnitude of the suppression of back-to-back jet-like two-particle correlations can be quantified with the ratio $I_{AA}(z_T) = D_{AA}(z_T)/D_{pp}(z_T)$. I_{AA}^{away} (bottom-left panel of Fig. 27) is found to decrease with increasing centrality, down to about 0.2–0.3 for the most central events [203, 212]. The right plot of Fig. 27 shows the best $\varepsilon_0 \approx 1.9$ GeV/fm value that fits the measured R_{AA} and I_{AA} factors. Due to the irreducible presence of (unquenched) partons emitted from the surface of the plasma, the leading hadron quenching factor $R_{AA}(p_T)$

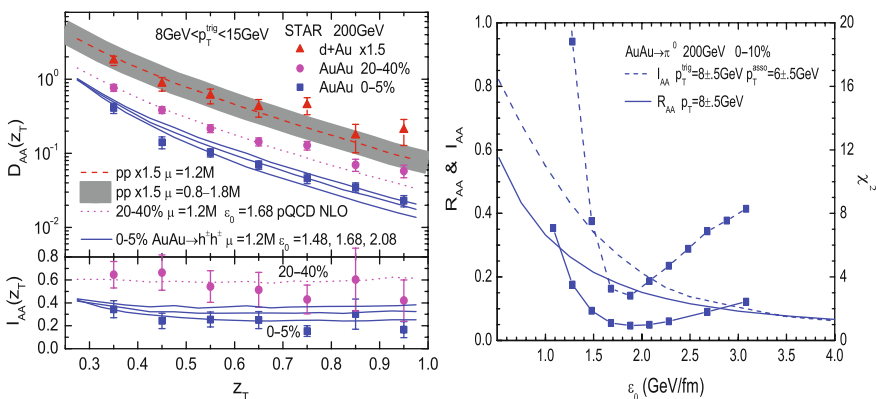


Fig. 27 Left: $D_{pp(AA)}^{\text{away}}(z_T)$ distributions for dAu and AuAu collisions at 200 GeV and $I_{AA}(z_T)$ ratio (for central AuAu) [212], compared to HT calculations [211] for varying ε_0 energy loss parameter. Right: Corresponding (data vs. theory) χ^2 values for the fitted ε_0 parameter [211]

is in general less sensitive to the value of ε_0 than the di-hadron modification ratio $I_{AA}(\zeta_T)$.

5.2 Azimuthal Correlations: Away-Side Broadening and “Conical” Emission

Since energy and momentum are conserved, the “missing” fragments of the away-side (quenched) parton at intermediate p_T 's must be either shifted to lower energy ($p_T \lesssim 2$ GeV/c) and/or scattered into a broadened angular distribution. Both softening and broadening are seen in the data when the p_T of the away-side associated hadrons is *lowered* (see two leftmost panels of Fig. 26). Figure 28 shows in detail the di-hadron azimuthal correlations $dN_{\text{pair}}/d\Delta\phi$ in central AuAu collisions [205, 213]: the away-side hemisphere shows a very unconventional angular distribution with a “dip” at $\Delta\phi \approx \pi$ and two neighbouring local maxima at $\Delta\phi \approx \pi \pm 1.1$ –1.4. Such a “volcano”-like profile has been interpreted as due to the preferential emission of energy from the quenched parton at a finite angle with respect to the jet axis. This could happen in a purely energy loss scenario due to large-angle radiation [214], but more intriguing explanations have been put forward based on the dissipation of the lost energy into a *collective* mode of the medium in the form of a wake of lower energy gluons with Mach- [44–48] or Čerenkov-like [48–51] angular emissions.

In the Mach cone scenario [44–48], the local maxima in central AuAu are caused by the Mach shock of the supersonic recoiling parton traversing the medium with a resulting preferential emission of secondary partons from the plasma at an angle θ_M (Fig. 29). Such a mechanism would give access, via Eq. (15), to the speed sound c_s of the traversed matter. In an expanding plasma, the speed of sound changes from $c_s = 1/\sqrt{3}$ (QGP) to $c_s \approx \sqrt{0.2}$ (hadron gas) through $c_s = 0$ (mixed phase). The

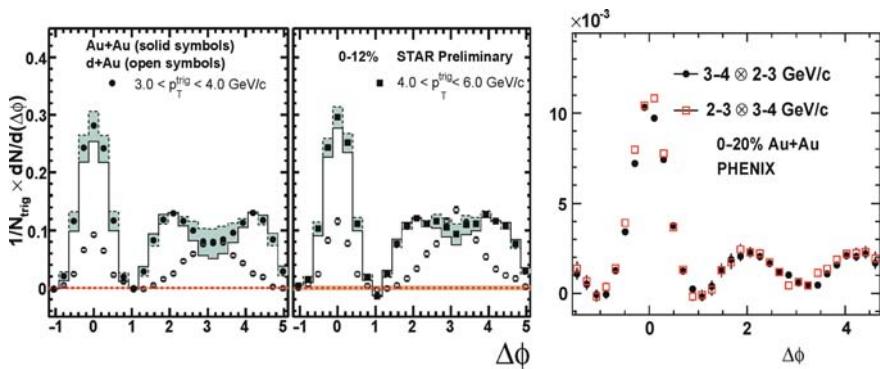


Fig. 28 Normalised azimuthal di-hadron distributions, $1/N_{\text{trig}} dN_{\text{pair}}/d\Delta\phi$. *Left*: STAR data in central AuAu (*squares*) and dAu (*circles*) for $p_T^{\text{assoc}} = 1.3$ –1.8 GeV/c and two ranges of p_T^{trig} [213]. *Right*: PHENIX results in central AuAu for various $p_T^{\text{trig,assoc}}$ ranges [209]

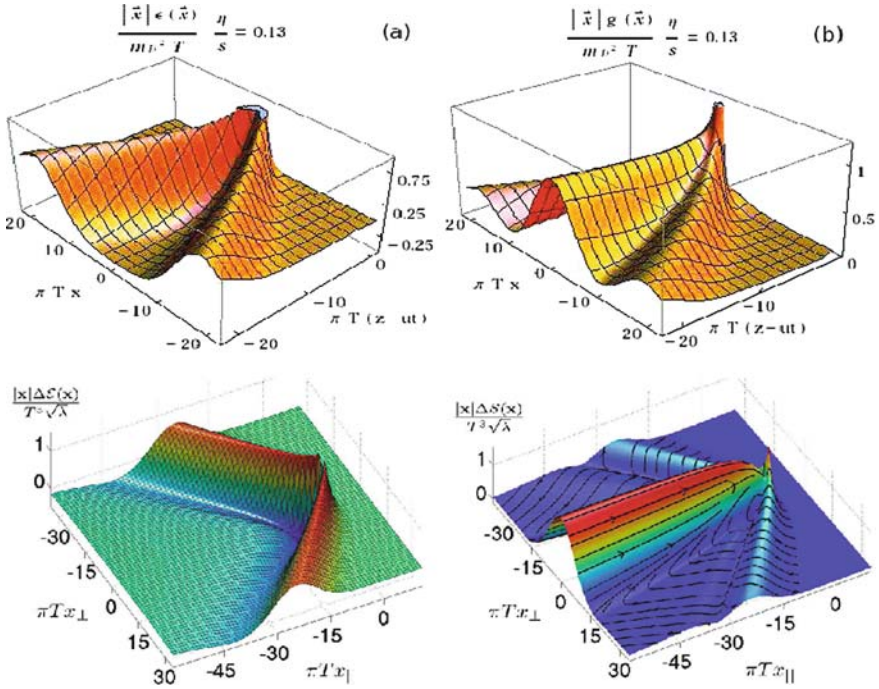


Fig. 29 *Top*: Perturbed energy (*left*) and momentum (*right*) densities for a gluon moving with $\beta = 0.99955$ in a perturbative QGP [220]. *Bottom*: Perturbed energy density (*left*) and energy flux (Pointing vector, *right*) for a jet with $\beta = 0.75$ from an AdS/CFT model [219]

time-averaged value is $\langle c_s \rangle = \frac{1}{\tau} \int_0^{\tau} dt c_s(t) \approx 0.3$ [46, 47] with a resulting Mach angle $\theta_M = \arccos(c_s) \approx 1.3$, in rough agreement with the experimental data.

In the Čerenkov picture [48–51], it is argued that the combination of the LPM gluonstrahlung interference and a medium with a *large* dielectric constant ($n \approx 2.75$ is needed in Eq. (16) to reproduce the location of the experimental peaks) should also result in the emission of QCD Čerenkov radiation with the double-hump structure observed in the data. However, at variance with the Mach angle which is constant in the fluid, the Čerenkov angle *decreases* with the momentum of the radiated gluon. Such a trend is seemingly in disagreement with the fact that the measured θ_c remains relatively constant as a function of p_T^{assoc} [209, 215]. In addition, STAR [216] and PHENIX [217] 3-particle correlation studies seem to clearly favour the *conical* over deflected-jets interpretation.

Theoretically, the disturbance of the energy-momentum tensor caused by a heavy quark has been studied in a $\mathcal{N} = 4$ SYM plasma [218, 219] as well as for a light quark in a perturbative plasma [220]. In both cases a clear conical structure as well as a strong flow generated along the path of the jet (diffusion wake [221–224]) are observed (Fig. 29). The results are sensitive to the viscosity of the medium. Yet, phenomenologically, it is unclear if such partonic collective wake(s) and cone survives both hadronisation and the final hadronic freeze-out [223–229]. Results for

a pQCD plasma [227] indicate that the conical signal does not survive freeze-out: a peak at $\Delta\phi = \pi$ appears due to the strong diffusion wake. More involved studies, accounting for, e.g. the plasma expansion and the hadronic phase, are needed before a final conclusion can be reached.

5.3 Pseudorapidity Correlations: Near-Side “Ridge”

Figure 30 shows the associated $\Delta\eta$ - $\Delta\phi$ particle yield ($p_T^{\text{assoc}} \gtrsim 20$ MeV/c) for trigger hadrons $p_T^{\text{trig}} > 2.5$ GeV/c in pp (PYTHIA simulations) and central AuAu (PHOBOS data) at 200 GeV. Both distributions show a clear peak at $(\Delta\eta, \Delta\phi) \approx (0, 0)$ as expected from jet fragmentation, but the near-side peak in heavy-ion collisions features a wide associated yield out to $\Delta\eta \approx 4$, referred to as the “ridge” [230]. The existence of such unique long-range rapidity correlations in the near side of the *trigger* parton which is, by construction, the least affected by the medium is puzzling. The properties (particle composition, p_T slope, intra-particle correlations) of this structure are very similar to those of the soft underlying event in the collision [231], clearly suggesting that the ridge is formed from bulk matter and not from jet fragments. Though many different interpretations have been put forward (see, e.g., [232] for a summary), models that do *not* require jet triggers for the effect to appear – such as, e.g. “glasma” flux tubes [233] or “trivial” modifications of the 2- and 3-particle correlations due to radial flow [232] – seem favoured.

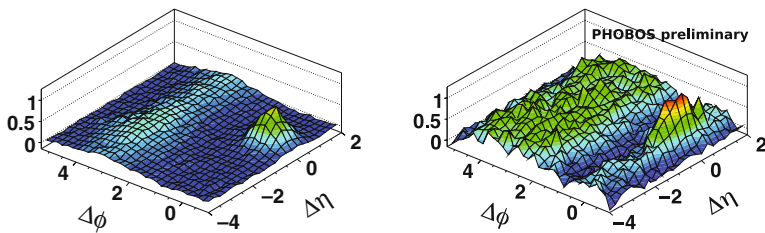


Fig. 30 Per-trigger associated hadron yield for $p_T^{\text{trig}} > 2.5$ GeV/c as a function of $\Delta\eta$ and $\Delta\phi$ for pp (PYTHIA, *left*) and 0–30% central AuAu (PHOBOS, *right*) collisions at 200 GeV [234]

6 Jet Observables in AA Collisions

The measurement of the leading fragments of a jet (single-hadron spectra and/or di-hadron azimuthal correlations at high- p_T) in AA collisions has been covered in detail in the previous sections. In this last chapter, we focus on *full jet* reconstruction in nuclear reactions. The study of the energy and particle-multiplicity distributions within a jet issuing from the fragmentation of quenched parton is a powerful tool to study the response of hot and dense QCD matter to fast quark and gluons.

6.1 Full Jet Reconstruction in AA Collisions

Experimental reconstruction of jets in hadronic and nuclear collisions is an involved exercise [235, 236] that requires at least three steps:

- *Clustering algorithm*: Hadrons belonging to a given jet are measured in the detector (usually in the cells of the hadronic and electromagnetic calorimeters) and are clustered together, according to relative “distances” in momentum and/or space, following an *infrared- and collinear-safe* procedure that can be also appropriately applied to “theoretical” (Monte Carlo) jets. The algorithm needs to be *fast* enough to be run over events with very high multiplicities. Various jet finders exist presently that fulfil all such conditions, e.g. k_T [237] and SIScone [238] as implemented in the FASTJET package [239].
- *Background subtraction*: Jets are produced on top of a large “underlying event” (UE) of hadrons coming from other (softer) parton–parton collisions in the same interaction. At LHC energies, extrapolating from $dE_T/d\eta|_{\eta=0} = 0.6$ TeV measured at RHIC [166, 167], one expects a total transverse energy of ~ 1 TeV in 1-unit rapidity at midrapidity. Jet reconstruction is usually carried out with small cone radius $R = \sqrt{\Delta\eta^2 + \Delta\phi^2} = 0.3\text{--}0.5$ (or similar k_T -distances, D) to minimise the UE contributions. Indeed, at the LHC in a $R = 0.4$ cone one expects $\Delta E_T = \pi \times R^2 \times 1/(2\pi) \times dE_T/d\eta|_{\eta=0} \approx 80$ GeV with large fluctuations. This observation already indicates that it will be challenging to reconstruct jets below $E_T \approx 50$ GeV. Various UE subtraction techniques have been developed in combination with the k_T [240–242], UA1-cone [242, 243], or iterative-cone [244] algorithms.
- *Jet corrections*: The energy of the reconstructed and background-subtracted jets has to be corrected for various experimental and model-dependent uncertainties before comparing it to theoretical predictions. Experimentally, the *jet energy scale* (JES) is the most important source of systematic uncertainties in the jet yield and requires careful data-driven studies (e.g. via dijet and γ -, Z-jet balancing in proton–proton collisions). In addition, before a given “parton-level” pQCD calculation can be compared to a measured “hadron-level” jet spectrum, one needs to estimate the non-perturbative effects introduced by the underlying-event and hadronisation corrections. In pp collisions, this final step is carried out usually comparing the results from two Monte Carlos (e.g. PYTHIA and HERWIG) with different models for the UE multiparton interactions as well as for the hadronisation (string and cluster-fragmentation, respectively).

6.2 Jet Clustering Algorithms

In practical terms one usually deals with three types of “jets” (Fig. 31, left). Experimentally, a *calorimeter jet* (aka “CaloJet”) is a collection of four vectors based on calorimeter towers clustered in pseudorapidity- azimuth according to a given algorithm. At the Monte Carlo generator level, a *hadron or particle jet* (aka “GenJet”) is

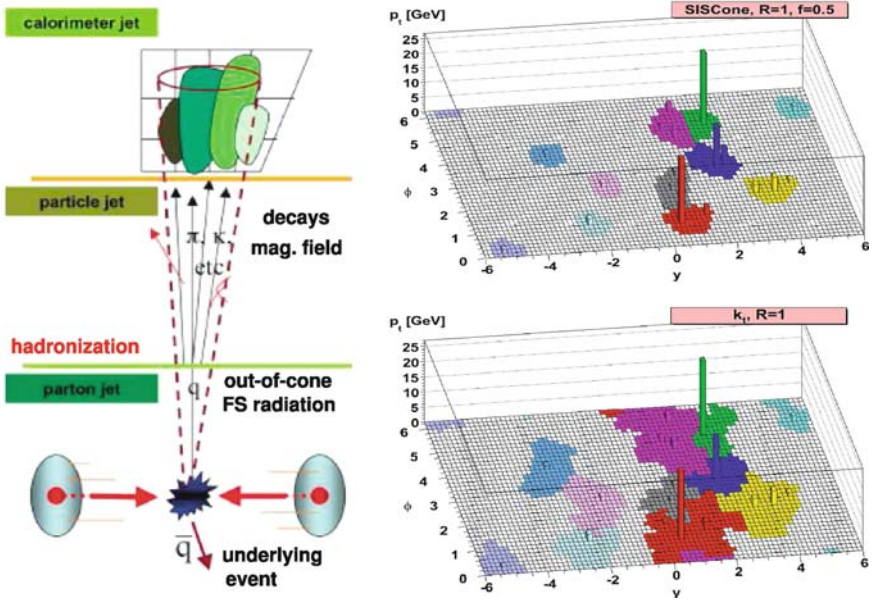


Fig. 31 *Left*: Schema of jet production and measurement [235]. *Right*: Reconstructed jets in η - ϕ space with the SIS Cone (*top*) and k_T (*bottom*) algorithms for a simulated pp event at the LHC [245]

a collection of hadrons issuing from the (non-perturbative) hadronisation of a given parton. Theoretically, a *parton-level jet* is what one actually calculates in pQCD. The (non-unique) method to link an initial parton to a set of final-state particles relies on a procedure known as “jet algorithm”.

The goal of a clustering algorithm is to combine hadrons into jets according to a given “distance” (radius). Theoretically, such a procedure must be *infrared* and *collinear safe* – i.e. adding a soft gluon or splitting a given parton must *not* change the final number of reconstructed jets. In addition, the jet finder must not be too sensitive to non-perturbative effects – hadronisation, underlying event (and pileup in pp) – and it must be realistically applicable at detector level (e.g. not too slow). There are two broad groups of jet algorithms [235, 236]:

- *Cone-type* algorithms are “top-down” approaches, i.e. they identify energy flow into pre-defined cones of a given radius. One sums the momenta of all particles j within a cone of radius R around a seed particle i (often the particle or calorimeter tower with the largest transverse momentum) in azimuthal angle ϕ and pseudorapidity η , i.e. taking all j such that

$$\Delta_{ij}^2 = (\eta_i - \eta_j)^2 + (\phi_i - \phi_j)^2 < R^2. \tag{47}$$

The direction of the resulting sum is then used as a new seed direction, and one iterates the procedure until the direction of the resulting cone is stable

(Fig. 31, top-right). There exist many flavours of this method developed (Jet-Clu, ILCA/MidPoint, ICone, SIScone, etc.) which have been mainly employed at hadron colliders. Their main advantages are their speed, which makes them easy to implement in triggers, and the simplicity of the UE corrections. On the other hand, their particular implementations can be messy (seeding, split–merge, dark towers, etc.) and infrared/collinear safety is not guaranteed in many cases.

- *Sequential clustering* algorithms are “bottom-up” approaches that rely on pairwise successive recombinations of the closest hadrons in momentum up to a given (predefined) distance D . One introduces distances d_{ij} between entities (particles, pseudojets) i and j , and d_{iB} between entity i and the beam (B). The clustering proceeds by identifying the smallest of the distances, and if it is a d_{ij} recombining entities i and j , while if it is d_{iB} calling i a jet and removing it from the list. The distances are recalculated and the procedure repeated until no entities are left. The distance measures for several algorithms are of the form

$$d_{ij} = \min(k_{T,i}^{2p}, k_{T,j}^{2p}) \frac{\Delta_{ij}^2}{D^2} \quad , \quad d_{iB} = k_{T,i}^{2p} \quad , \quad (48)$$

where Δ_{ij}^2 is defined in Eq. (47), $k_{T,i}$ is the transverse momentum of particle i , D is the jet-radius parameter, and p parameterises the type of algorithm: k_T ($p = 1$) [246], Cambridge/Aachen ($p = 0$) [247], anti- k_T ($p = -1$) [245] (Fig. 31, bottom-right). On the positive side, these algorithms – widely used at LEP and HERA – are explicitly infrared and collinear safe and more “realistic” than the cone-based ones as they mimic (backwards) the QCD shower branching dynamics. On the other hand, they used to be slow and the UE subtraction trickier compared to the cone jet finders, making them not competitive in a heavy-ion environment with very large hadron multiplicities. Recently, the time taken to cluster N particles has been significantly improved in the FASTJET [239] implementation, based on Voronoi diagrams, going down from $\mathcal{O}(N^3)$ for the default k_T jet finder to $\mathcal{O}(N \ln N)$. Jet clustering in nucleus–nucleus collisions is now routinely performed at sub-second times.

6.3 Underlying Event Subtraction

Background energy in a jet cone of size R is $\mathcal{O}(R^2)$ and background fluctuations are $\mathcal{O}(R)$. As aforementioned, the soft background from the underlying event in a cone of $R = 0.4$ in central nucleus–nucleus collisions at RHIC (LHC) is about 40 (80) GeV. Figure 32 (left) shows the (charged) jet and background energies as a function of the cone radius R in ALICE [174, 241]. Jets can only be identified if the background energy within the cone is smaller than the signal energy. This can be achieved by decreasing the cone size ($E_T^{\text{bgd}} \propto R^2$) to $R = 0.3$ – 0.5 and by applying p_T or energy cuts on the charged hadrons or calorimeter towers. The latter option is not optimal since it also introduces potential biases in the measurement of jet

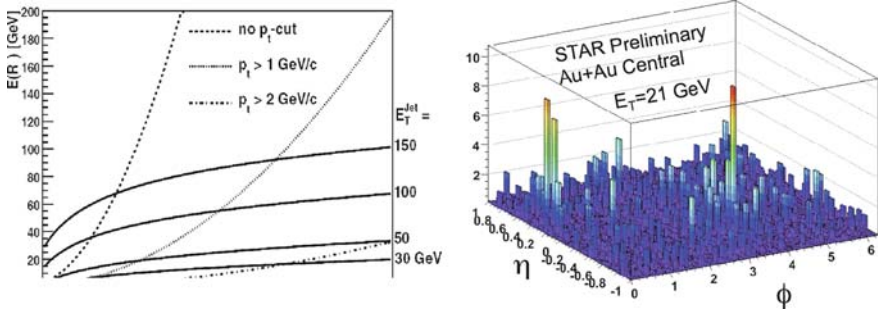


Fig. 32 *Left*: Charged jet energy in a cone of radius R (full lines) in ALICE compared to the background energy from a HIJING [248] simulation for different cuts in the particles p_T (dashed lines) [174]. *Right*: STAR AuAu dijet event after background subtraction [249, 250]

quenching effects. STAR [249, 250] (Fig. 32, right) uses a seeded-cone algorithm with $R = 0.4$ and $p_T^{cut} = 0.1 - 2$ GeV/c and estimates the UE background event by event from the average energy in cones without seeds which is then subtracted from the reconstructed jets. ALICE uses a modified version of the UA1-cone algorithm ($R = 0.4$) where the mean cell energy from cells outside a jet cone is recalculated after each iteration of the cone jet finder and subtracted from all cells [174, 241].

Similarly, CMS [244, 176] subtracts the UE on an event-by-event basis with a variant of the iterative “noise/pedestal subtraction” for pp collisions [251]. Initially, the mean value and dispersion of the energies in the calorimeter cells are calculated for rings of constant pseudorapidity, η . The value of this pedestal function, $P(\eta)$, is subtracted from all cells (the cell energy is set to zero in case of negative values) and the jets are reconstructed with the default I Cone finder. In a second iteration, the pedestal function is recalculated using only calorimeter cells outside the area covered by jets with $E_T > 30$ GeV. The cell energies are updated with the new pedestal function and the jets are reconstructed again, using the updated calorimeter cells.

Alternatively, FASTJET [240] proposes a background-subtraction procedure *after* running any infrared-safe algorithm. The method is based on the concept of a “jet area” A constructed by adding infinitely soft particles (“ghosts”) and identifying the region in η, ϕ where those ghosts are clustered within each jet [241]. Each reconstructed jet p_T is then corrected by subtracting the median value of the noise distribution in the event, $\rho = \text{median}[\{p_T/A\}]$, in the jet area A , via $p_T^{\text{sub}} = p_T - A \cdot \rho$. In practical terms, one fits the measured $p_T(\eta)/A$ background distribution for each event with a parabola form, $\rho(\eta) = a + b\eta^2$ (which excludes any jet peak) and corrects then the jet p_T using the formula above.

6.4 Jet Corrections

The last step of any jet analysis consists in correcting the p_T of any measured *Calo-Jet* to match closely that of the associated *GenJet* or *parton-level* jet, so that it can be

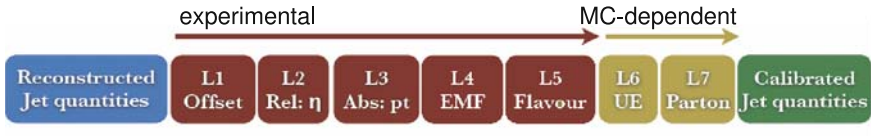


Fig. 33 List of typical factorised jet energy corrections (CMS analysis) [251]

compared to theoretical expectations. In principle, the different corrections can be decomposed as shown in Fig. 33. The experimental corrections (labelled levels 1–5 in the plot) can be extracted from the data themselves. For example, the correction L1 (noise offset) can be obtained from minimum-bias events *without* jet activity, and the L2 (flattening of relative, η -dependent, p_T responses of the calorimeters) and L3 (absolute p_T calibration) can be derived using p_T -balancing techniques in back-to-back dijet and γ -, Z -jet events in pp collisions. A precise calibration of the jet energy scale (JES) is essential. Given the steep (power law) fall-off of the jet cross section as a function of energy, an uncertainty of 10% in the JES can propagate into uncertainties as large as 50% in the jet yield at a given p_T bin. The L3 correction is thus the most important source of experimental uncertainty in any jet measurement. The two last corrections, L4 (fraction EMF of energy deposited by hadrons in the EM calorimeter) and L5 (flavour correction accounting for the different characteristics of – and therefore detector responses to – gluon, light-quark, and heavy-quark jets) can be, e.g. obtained in back-to-back γ -jet and b,c -identified dijet events in pp .

The two “theoretical” corrections (L6 – UE and L7 – parton) aim at bringing the p_T of a *CaloJet* as close as possible to that of its originating parton. They can only be obtained from MC simulations that model the effects of final-state radiation (FSR), hadronisation, and underlying event. In pp collisions, the total shift on a jet p_T can be approximated by the uncorrelated sum $\langle \delta p_T^2 \rangle \approx \langle \delta p_T \rangle_{\text{FSR}}^2 + \langle \delta p_T \rangle_{\text{hadr}}^2 + \langle \delta p_T \rangle_{\text{UE}}^2$. FSR and hadronisation tend to remove energy out of the jet cone, whereas the UE has the contrary “splash-in” effect [252]. The way these effects modify the jet energy as a function of the parton p_T , flavour and the used cone radius R are summarised in Table 3. Whereas the effect of FSR can be in principle computed perturbatively, the UE and hadronisation corrections rely on model-dependent descriptions of multi-parton interactions (MPI) and parton fragmentation. In pp collisions, one usually compares the result of PYTHIA and HERWIG – which have different MPI and dif-

Table 3 Main physical effects that contribute to a shift $\langle \delta p_T \rangle$ between the transverse momentum of a jet and its parent parton in pp collisions (cases with “–” do not have any dependence at LO) [252]

	Dependence of jet $\langle \delta p_T \rangle$ shift on		
	Parton p_T	Colour factor	Radius R
Final-state radiation	$\sim \alpha_s(p_T) p_T$	C_i	$\ln R + \mathcal{O}(1)$
Hadronisation	–	C_i	$-1/R + \mathcal{O}(R)$
Underlying event	–	–	$R^2/2 + \mathcal{O}(R^4)$

ferent (string vs. cluster) fragmentation models – to gauge the dependence of the measured jet observables on these non-perturbative phenomena.

In heavy-ion collisions, in-medium FSR and UE are significantly enhanced compared to pp jets, but, since hadronisation occurs after traversing the medium, the final parton-to-hadron fragmentation should be the same as in the vacuum. Ideally, the effects of the UE can be controlled embedding MC jets in real events, and the influence of hadronisation can be gauged, e.g. comparing the results of Q-PYTHIA and Q-HERWIG [40]. Jet quenching observables – which are the ultimate goal of our studies – can then be isolated comparing the results of different parton energy loss MCs such as, e.g. PYQUEN (with large out-of-cone elastic energy loss) and Q-PYTHIA (with its embedded BDMPS radiative energy loss).

6.5 Jet Shapes

The study of the internal structure of jets – via observables such as jet shapes and jet multiplicity distributions – in $p\bar{p}$ collisions at Tevatron has provided valuable tests of the models for parton branching and soft-gluon emission in the vacuum [253]. The energy degradation of partons traversing a dense QCD plasma will be also directly reflected in the modification of such jet observables in heavy-ion collisions. Two variables are useful in this context:

- the *differential jet shape*, $\rho(r)$, is the average fraction of the jet p_T that lies inside an annulus of radius $r \pm \delta r/2$ around the jet axis (e.g. $\delta r = 0.1$):

$$\rho(r) = \frac{1}{\delta r} \frac{1}{N_{\text{jet}}} \sum_{\text{jets}} \frac{p_T(r - \delta r/2, r + \delta r/2)}{p_T(0, R)}, \quad 0 \leq r = \sqrt{\Delta y^2 + \Delta \phi^2} \leq R, \quad (49)$$

- the *integrated jet shape*, $\Psi(r)$, is the average fraction of the jet p_T that lies inside a cone of radius r concentric to the jet cone (by definition, $\Psi(r = R) = 1$):

$$\Psi(r) = \frac{1}{N_{\text{jet}}} \sum_{\text{jets}} \frac{p_T(0, r)}{p_T(0, R)}, \quad 0 \leq r \leq R. \quad (50)$$

Medium-modified jet shapes in $PbPb$ collisions at LHC energies have been analytically investigated in [38, 54]. More detailed studies using the recently available jet quenching Monte Carlos (see Sect. 3.3) are needed.

6.6 Medium-Modified Fragmentation Functions

Due to the coherence and interference of gluon radiation *inside* a jet (resulting, on average, in *angular ordering* of the sequential branching), not the softest partons but those with intermediate energies ($E_h \propto E_{\text{jet}}^{0.3-0.4}$) multiply most effectively in QCD cascades [254]. This is best seen in the approximately Gaussian distribution

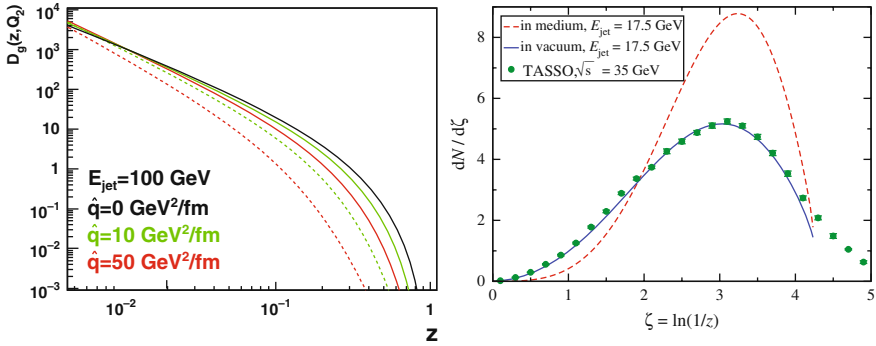


Fig. 34 *Left*: Medium-modified pion fragmentation function for a 100-GeV gluon going through a medium with increasing \hat{q} parameter [56]. *Right*: Single inclusive distribution of hadrons vs. $\xi = \ln(E_{\text{jet}}/p)$ for a 17.5-GeV jet in e^+e^- collisions (TASSO data) compared to MLLA predictions in the vacuum (solid curve) and in-medium (dashed curve) [39]

in the variable $\xi = \log(E_{\text{jet}}/p) = \log(1/z)$ for particles with momentum p in a jet of energy E_{jet} , which peaks at the so-called humpback plateau at intermediate $\xi \approx 3-4$ values (Fig. 34, right). As discussed previously, energy loss in a QCD medium shifts parton energy from high- z to low- z hadrons. As a result, leading hadrons are suppressed as seen in Fig. 34 (left) where, for increasing \hat{q} coefficient, the fragmentation function $D_{i \rightarrow h}(z, Q^2)$ is depleted at high- z . Correspondingly, the number of low- p_T hadrons increases, as seen by the *higher* humped back in Fig. 34 (*right*).

Theoretically, the resummed (next-to) modified leading logarithmic approximation (N)MLLA approach describes well, to (next-to)-next-to-leading order $\sqrt{\alpha_s}$ accuracy, the measured distributions of hadrons $D_{i \rightarrow h}(z, Q^2)$ inside a jet (Fig. 34, right) down to non-perturbative scales $Q_{\text{eff}} \approx \Lambda_{\text{QCD}} \approx 200$ MeV, provided that each parton is mapped locally onto a hadron (“Local Parton–Hadron Duality”, LPHD) [255] with a proportionality factor $\kappa \approx 1$. Various recent promising applications of the (N)MLLA approach [256, 57, 41, 42] have investigated QCD radiation in the presence of a medium.

6.7 Photon-Jet Correlations

The γ -jet (and Z -jet) channel provides a very clean means to determine parton fragmentation functions (FFs) [257]. In the dominant QCD Compton process of photon production ($qg \rightarrow q\gamma$), because of momentum conservation the photon is produced back to back to the hard quark, with equal and opposite transverse momentum. Since the prompt γ is not affected by final-state interactions, its transverse energy (E_T^γ) can be used as a proxy of the away-side parton energy ($E_T^{\text{jet}} \approx E_T^\gamma$) *before* any jet quenching has taken place in the medium. Once the quark fragments into a hadron h , the γ - h momentum imbalance variable [52], $z_{\gamma h} \equiv -\mathbf{p}_{T,h} \cdot \mathbf{p}_{T,\gamma} / |\mathbf{p}_{T,\gamma}|^2$, reduces

at LO to the fragmentation variable, $z_{\gamma h} = z$. The FF, defined as the normalised distribution of hadron momenta $1/N_{\text{jets}} dN/dz$ relative to that of the parent parton E_T^{jet} , can be constructed using $z_{\gamma h}$ or, similarly, $\xi = -\ln(z_{\gamma h})$, for all particles with momentum p_T associated with the jet.

ALICE [242, 258] and CMS [259] have carried out simulation studies of the γ -jet channel, where the isolated γ is identified in ECAL, the away-side jet *axis* ($\Delta\phi_{\gamma\text{-jet}} > 3$ rad) is reconstructed in the calorimeters, and the momenta of hadrons around the jet axis ($R_{\text{jet}} < 0.5$) are measured in the tracker. In the CMS acceptance and for $E_T^\gamma > 70$ GeV, about 4500 γ -jet events are expected according to PYTHIA (scaled by the Glauber nuclear overlap) in one PbPb year at the nominal luminosity. The obtained FFs for photon-jet events – after subtraction of the underlying-event tracks – are shown in Fig. 35 for central PbPb. Medium-modified FFs are measurable with high significance in the ranges $z < 0.7$ and $0.2 < \xi < 6$.

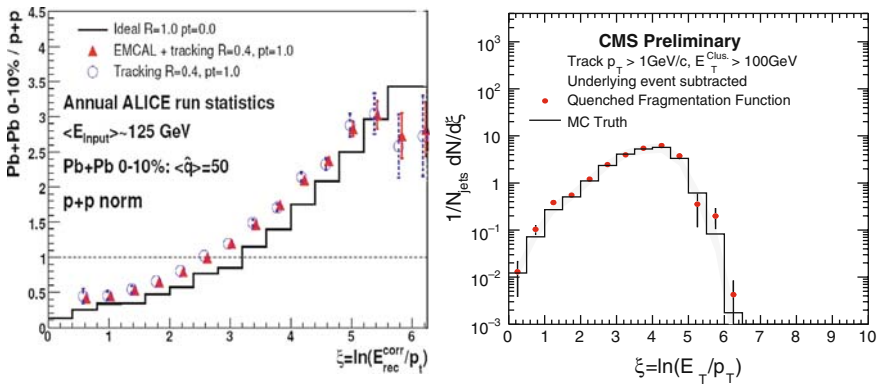


Fig. 35 Medium-modified FF (*right*) and ratio FF(med)/FF(vac) (*left*) as a function of ξ for quenched partons obtained in γ -jet simulations for central PbPb at 5.5 TeV (0.5 nb^{-1}) in ALICE (*left*) [242, 258] and CMS (*right*) [259]

7 Summary

We have reviewed the main theoretical motivations behind the experimental study of parton scattering and jet fragmentation in the hot and dense QCD matter created in high-energy nucleus–nucleus collisions. The phenomenology of parton energy loss has been summarised as well as the main experimental results on single inclusive spectra and di-hadron correlations measured at high transverse momentum, mainly in AuAu reactions at RHIC collider energies ($\sqrt{s_{NN}} = 200$ GeV). The “tomographic” analysis of jet structure modifications in AA collisions provides quantitative information on the thermodynamical and transport properties of the strongly interacting medium produced in the reactions. Two notable experimental results have been discussed in detail: (i) the observed factor ~ 5 suppression of

high- p_T leading hadrons and (ii) the strongly distorted azimuthal distributions of secondary hadrons emitted in the away-side hemisphere of a high- p_T trigger hadron, in central AuAu relative to pp collisions in free space. Most of the properties of the observed high- p_T single hadron and di-hadron suppression (such as its magnitude, light flavour “universality”, p_T , reaction centrality, path-length, and $\sqrt{s_{NN}}$ dependences) are in quantitative agreement with the predictions of parton energy loss models. The confrontation of these models to the data permits to derive the initial gluon density $dN^g/dy \approx 1400$ and transport coefficient $\langle \hat{q} \rangle \approx 13 \text{ GeV}^2/\text{fm}$ of the produced medium at RHIC.

In the last section of this document, we have reviewed the details of jet reconstruction in heavy-ion collisions: jet algorithms, underlying-event background subtraction, and jet energy corrections. The analysis of jet shapes and the extraction of medium-modified parton-to-hadron fragmentation functions at low- and high-hadron momenta promise to shed more light onto the mechanisms of parton energy loss in QCD matter at the coming LHC energies. The study of jet quenching phenomena is significantly expanding our knowledge of the dynamics of the strong interaction at extreme conditions of temperature and density.

Acknowledgments DdE would like to thank Sourav Sarkar, Helmut Satz, and Bikash Sinha for their kind invitation to lecture at the 2008 Jaipur QGP Winter School and for the excellent atmosphere and hospitality at the school. DdE acknowledges support by the 6th EU Framework Programme contract MEIF-CT-2005-025073. The work of B.B. is supported by BMBF and by the Helmholtz Research School H-QM.

References

1. D. d'Enterria: J. Phys. **G 34**, S53 (2007) 285, 286
2. See e.g. F. Karsch and E. Laermann: arXiv:hep-lat/0305025 285, 306
3. E.V. Shuryak: Sov. Phys. JETP **47**, 212 (1978) 285
4. E.V. Shuryak: Zh. Eksp. Teor. Fiz. **74**, 408 (1978)
5. J.C. Collins and M.J. Perry: Phys. Rev. Lett. **34**, 1353 (1975)
6. B.A. Freedman and L.D. McLerran: Phys. Rev. **D 16**, 1169 (1977) 285
7. A. Accardi et al.: arXiv:hep-ph/0310274 287
8. V.N. Gribov and L.N. Lipatov: Sov. J. Nucl. Phys. **15**, 438 (1972) 287
9. V.N. Gribov and L.N. Lipatov: Yad. Fiz. **15**, 781 (1972)
10. G. Altarelli and G. Parisi: Nucl. Phys. **B 126**, 298 (1977)
11. Y.L. Dokshitzer: Sov. Phys. JETP **46**, 641 (1977)
12. Y.L. Dokshitzer: Zh. Eksp. Teor. Fiz. **73**, 1216 (1977) 287, 292
13. J.D. Bjorken: FERMILAB-PUB-82-059-THY (1982) 287, 292
14. P. Arnold: arXiv:0808.2767 [hep-ph] 288, 304
15. P. Arnold and W. Xiao: arXiv:0810.1026 [hep-ph]
16. R. Baier and Y. Mehtar-Tani: arXiv:0806.0954 [hep-ph] 288
17. R. Baier and D. Schiff: JHEP **0609**, 059 (2006) 288
18. S. Peigné and A.V. Smilga: arXiv:0810.5702 [hep-ph] 290, 291, 294
19. W.M. Yao et al. [Particle Data Group]: J. Phys. **G 33**, 1 (2006) 290
20. A.B. Migdal: Phys. Rev. **103**, 1811 (1956) 291
21. A. Peshier: Phys. Rev. Lett. **97**, 212301 (2006) 291, 292, 319
22. S. Peigné and A. Peshier: Phys. Rev. **D 77**, 114017 (2008) 291, 292, 319

23. R.K. Ellis, W.J. Stirling and B.R. Webber: *QCD and Collider Physics*, Camb. Monogr. Part. Phys. Nucl. Phys. Cosmol. **8**, 1 (1996) 291
24. E. Braaten and M.H. Thoma: Phys. Rev. **D 44**, 2625 (1991) 292
25. B.G. Zakharov: JETP Lett. **86**, 444 (2007) 292
26. M. Gyulassy and M. Plümer: Phys. Lett. **B243**, 432 (1990) 292, 294, 307
27. X.N. Wang, M. Gyulassy: Phys. Rev. Lett. **68**, 1480 (1992) 294, 307
28. R. Baier, Y.L. Dokshitzer, A.H. Mueller, S. Peigné and D. Schiff: Nucl. Phys. **B484**, 265 (1997)
29. R. Baier, D. Schiff and B.G. Zakharov: Ann. Rev. Nucl. Part. Sci. **50**, 37 (2000)
30. M. Gyulassy, P. Levai and I. Vitev: Phys. Rev. Lett. **85**, 5535 (2000) 295
31. M. Gyulassy, P. Levai and I. Vitev: Nucl. Phys. **B594**, 371 (2001) 295
32. U.A. Wiedemann: Nucl. Phys. **B 588**, 303 (2000) 292, 299, 300
33. Y.L. Dokshitzer and D.E. Kharzeev: Phys. Lett. **B 519**, 199 (2001) 294
34. G.Y. Qin et al.: Phys. Rev. Lett. **100**, 072301 (2008) 293
35. S. Wicks, W. Horowitz, M. Djordjevic and M. Gyulassy: Nucl. Phys. **A 784**, 426 (2007) 293, 299, 301
36. D.A. Appel: Phys. Rev. **D 33**, 717 (1986) 294
37. J.P. Blaizot and L.D. McLerran: Phys. Rev. **D 34**, 2739 (1986) 294
38. C.A. Salgado and U.A. Wiedemann: Phys. Rev. Lett. **93**, 042301 (2004) 294, 296, 331
39. N. Borghini and U.A. Wiedemann: arXiv:hep-ph/0506218 296, 305, 332
40. N. Armesto, L. Cunqueiro and C.A. Salgado: arXiv:0809.4433 [hep-ph] 296, 305, 331
41. R. Perez-Ramos: arXiv:0811.2418 [hep-ph] 332
42. R. Perez-Ramos: arXiv:0811.2934 [hep-ph] 332
43. S. Kretzer: Acta Phys. Polon. **B 36**, 179 (2005) 294
44. H. Stoecker: Nucl. Phys. **A750**, 121 (2005) 295, 323
45. L.M. Satarov, H. Stoecker and I.N. Mishustin: Phys. Lett. **B 627**, 64 (2005)
46. J. Casalderrey-Solana, E.V. Shuryak and D. Teaney: J. Phys. Conf. Ser. **27**, 22 (2005) 324
47. J. Casalderrey-Solana, E.V. Shuryak and D. Teaney: Nucl. Phys. **A 774**, 577 (2006) 324
48. J. Ruppert and B. Muller: Phys. Lett. **B618**, 123 (2005) 295, 323, 324
49. I.M. Dremin: Nucl. Phys. **A 767**, 233 (2006)
50. A. Majumder and X.N.Wang: nucl-th/0507062
51. V. Koch, A. Majumder and X.N. Wang: nucl-th/0507063 295, 323, 324
52. F. Arleo, P. Aurenche, Z. Belghobsi and J.P. Guillet: JHEP **0411**, 009 (2004) 295, 332
53. I.P. Lokhtin, A.V. Sherstnev and A.M. Snigirev: Phys. Lett. **B 599**, 260 (2004) 295
54. I. Vitev, S. Wicks and B.W. Zhang: arXiv:0810.2807 [hep-ph] 296, 331
55. F. Arleo: arXiv:0810.1193 [hep-ph] 296, 299
56. N. Armesto, L. Cunqueiro, C.A. Salgado and W.C. Xiang: JHEP **0802**, 048 (2008) 296, 305, 332
57. N. Armesto, C. Pajares and P. Quiroga-Arias: arXiv:0809.4428 [hep-ph] 296, 332
58. J.C. Collins, D.E. Soper and G. Sterman: Nucl. Phys. **B 261**, 104 (1985) 296
59. See e.g. D. d'Enterria: nucl-ex/0302016 298
60. A. Majumder: J. Phys. **G 34**, S377 (2007) 299
61. B.G. Zakharov: JETP Lett. **63**, 952 (1996) 299
62. B.G. Zakharov: JETP Lett. **65**, 615 (1997)
63. B.G. Zakharov: Phys. Atom. Nucl. **61**, 838 (1998)
64. B.G. Zakharov: Yad. Fiz. **61**, 924 (1998)
65. R. Baier, Y.L. Dokshitzer, A.H. Müller, S. Peigné and D. Schiff: Nucl. Phys. **B 483**, 291 (1997) 299
66. R. Baier, Y.L. Dokshitzer, A.H. Müller, S. Peigné and D. Schiff: Nucl. Phys. **B 484**, 265 (1997) 299, 300
67. U.A. Wiedemann: Nucl. Phys. **B 582**, 409 (2000) 299
68. C.A. Salgado and U.A. Wiedemann: Phys. Rev. Lett. **89**, 092303 (2002) 299, 300
69. C.A. Salgado and U.A. Wiedemann: Phys. Rev. **D 68**, 014008 (2003) 299, 300
70. M. Gyulassy, P. Levai and I. Vitev: Nucl. Phys. **B 571**, 197 (2000) 299, 301
71. M. Gyulassy, P. Levai and I. Vitev: Nucl. Phys. **B 594**, 371 (2001) 301

72. M. Gyulassy, P. Levai and I. Vitev: Phys. Lett. **B 538**, 282 (2002) 301
73. M. Djordjevic and M. Gyulassy: Nucl. Phys. **A 733**, 265 (2004) 299, 301
74. X.F. Guo and X.N. Wang: Phys. Rev. Lett. **85**, 3591 (2000) 299, 302, 313
75. X.N. Wang and X.F. Guo: Nucl. Phys. **A 696**, 788 (2001)
76. B.W. Zhang and X.N. Wang: Nucl. Phys. **A 720**, 429 (2003) 302
77. A. Majumder, E. Wang and X.N. Wang: Phys. Rev. Lett. **99**, 152301 (2007)
78. A. Majumder and B. Muller: Phys. Rev. **C 77**, 054903 (2008)
79. A. Majumder, R.J. Fries and B. Muller: Phys. Rev. **C 77**, 065209 (2008) 299
80. P. Arnold, G.D. Moore and L.G. Yaffe: JHEP **0111**, 057 (2001) 299, 303
81. P. Arnold, G.D. Moore and L.G. Yaffe: JHEP **0011**, 001 (2000)
82. S. Jeon and G.D. Moore: Phys. Rev. **C 71**, 034901 (2005) 303, 314
83. S. Turbide, C. Gale, S. Jeon and G.D. Moore: Phys. Rev. **C 72**, 014906 (2005) 299, 303, 310
84. R. Baier, Y.L. Dokshitzer, A.H. Müller and D. Schiff: Phys. Rev. **C 58**, 1706 (1998) 299
85. R. Baier, Y.L. Dokshitzer, A.H. Müller and D. Schiff: Nucl. Phys. **B 531**, 403 (1998) 299
86. R. Baier: Nucl. Phys. **A 715**, 209 (2003) 300, 301
87. U.A. Wiedemann: Nucl. Phys. **A 690**, 731 (2001) 300
88. N. Armesto, C.A. Salgado and U.A. Wiedemann: Phys. Rev. **D 69**, 114003 (2004) 300
89. A. Dainese, C. Loizides and G. Paic: Eur. Phys. J. **C 38**, 461 (2005) 300, 310, 311, 314, 315
90. C. Loizides: Eur. Phys. J. **C 49**, 339 (2007) 300, 315
91. M. Gyulassy and X.N. Wang: Nucl. Phys. **B 420**, 583 (1994) 301
92. M. Gyulassy, P. Levai and I. Vitev: Phys. Rev. Lett. **85**, 5535 (2000) 301
93. I. Vitev: J. Phys. Conf. Ser. **50**, 119 (2006) 301
94. J.W. Qiu and G. Sterman: Nucl. Phys. **B 353**, 105 (1991) 302
95. J.W. Qiu and G. Sterman: Nucl. Phys. **B 353**, 137 (1991)
96. M. Luo, J.W. Qiu and G. Sterman: Phys. Rev. **D 50**, 1951 (1994) 302
97. A. Majumder and X.N. Wang: arXiv:0806.2653 [nucl-th] 302
98. P. Arnold, G.D. Moore and L.G. Yaffe: JHEP **0112**, 009 (2001) 303
99. P. Arnold, G.D. Moore and L.G. Yaffe: JHEP **0206**, 030 (2002) 303
100. A. Adare et al. [PHENIX Collaboration]: Phys. Rev. Lett. **101**, 232301 (2008) 304, 309, 310, 311, 312, 315
101. S.A. Bass et al.: arXiv:0805.3271 [nucl-th] 304, 305
102. K. Eskola, H. Honkanen, C. Salgado and U. Wiedemann: Nucl. Phys. **A 747**, 511 (2005) 305, 307, 314
103. K. Zapp, G. Ingelman, J. Rathsmann, J. Stachel and U.A. Wiedemann: arXiv:0804.3568 305
104. S. Domdey, G. Ingelman, H.J. Pirner, J. Rathsmann, J. Stachel and K. Zapp: arXiv:0802.3282 [hep-ph]
105. T. Renk: Phys. Rev. **C 78**, 034908 (2008) 305
106. T. Sjostrand, S. Mrenna and P. Skands: JHEP **0605**, 026 (2006) 305
107. G. Corcella et al.: arXiv:hep-ph/0210213 305
108. I.P. Lokhtin and A.M. Snigirev: Eur. Phys. J. **C 45**, 211 (2006) 305
109. I.P. Lokhtin, L.V. Malinina, S.V. Petrushanko, A.M. Snigirev, I. Arsene and K. Tywoniuk: arXiv:0810.2082 [hep-ph] 305
110. E. Shuryak: Prog. Part. Nucl. Phys. **53**, 273 (2004) 306
111. T.D. Lee: Nucl. Phys. **A 750**, 1 (2005)
112. M. Gyulassy and L. McLerran: Nucl. Phys. **A 750**, 30 (2005) 306
113. J.M. Maldacena: Adv. Theor. Math. Phys. **2**, 231 (1998) 306
114. J.M. Maldacena: Int. J. Theor. Phys. **38**, 1113 (1999)
115. E. Witten: Adv. Theor. Math. Phys. **2**, 505 (1998) 306
116. K. Kajantie, T. Tahkokallio and J.T. Yee: JHEP **0701**, 019 (2007) 306
117. P. Kovtun, D.T. Son and A.O. Starinets: Phys. Rev. Lett. **94**, 111601 (2005) 306
118. H. Liu, K. Rajagopal and U.A. Wiedemann: Phys. Rev. Lett. **97**, 182301 (2006) 306
119. C.P. Herzog, A. Karch, P. Kovtun, C. Kozcaz and L.G. Yaffe: JHEP **0607**, 013 (2006) 306, 307, 319
120. J. Casalderrey-Solana and D. Teaney: Phys. Rev. **D 74**, 085012 (2006) 307
121. J. Casalderrey-Solana and D. Teaney: JHEP **0704**, 039 (2007)
122. S.S. Gubser: Phys. Rev. **D 74**, 126005 (2006) 306, 307, 319

123. H. Liu, K. Rajagopal and U.A. Wiedemann: JHEP **0703**, 066 (2007) 306
124. J. Casalderrey-Solana and C.A. Salgado: Acta Phys. Polon. **B 38**, 3731 (2007) 306, 307
125. B.I. Abelev et al. [STAR Collaboration]: Phys. Rev. Lett. **97**, 252001 (2006) 307, 308
126. J. Adams et al. [STAR Collaboration]: Phys. Rev. Lett. **91**, 172302 (2003) 307, 308, 310, 311
127. S.S. Adler et al. [PHENIX Collaboration]: Phys. Rev. Lett. **91**, 241803 (2003) 307, 308
128. S.S. Adler et al. [PHENIX Collaboration]: Phys. Rev. Lett. **98**, 012002 (2007) 307
129. A. Adare et al. [PHENIX Collaboration]: Phys. Rev. Lett. **97**, 252002 (2006) 307, 308
130. I. Arsene et al. [BRAHMS Collaboration]: Phys. Rev. Lett. **93**, 242303 (2004) 307, 308
131. F. Aversa, P. Chiappetta, M. Greco and J.P. Guillet: Nucl. Phys. **B 327**, 105 (1989) 307, 308, 309, 310, 317, 318
132. B. Jager, A. Schafer, M. Stratmann and W. Vogelsang: Phys. Rev. **D 67**, 054005 (2003)
133. W. Vogelsang (private communication) 309, 310, 317, 318
134. L.E. Gordon and W. Vogelsang: Phys. Rev. **D 48**, 3136 (1993)
135. L.E. Gordon: Phys. Rev. **D 50**, 6753 (1994)
136. W. Vogelsang (private communication)
137. P. Aurenche, A. Douiri, R. Baier, M. Fontannaz and D. Schiff: Phys. Lett. **B 140**, 87 (1984)
138. P. Aurenche, R. Baier, M. Fontannaz and D. Schiff: Nucl. Phys. **B 297**, 661 (1988) 307, 308
139. M. Cacciari, P. Nason and R. Vogt: Phys. Rev. Lett. **95**, 122001 (2005) 307, 308
140. J. Pumphlin, D.R. Stump, J. Huston, H.L. Lai, P.M. Nadolsky and W.K. Tung: JHEP **0207**, 012 (2002) 307
141. B.A. Kniehl, G. Kramer and B. Potter: Nucl. Phys. **B 597**, 337 (2001) 307
142. S. Kretzer: Phys. Rev. **D 62**, 054001 (2000) 307
143. S.S. Adler et al. [PHENIX Collaboration]: Phys. Rev. Lett. **91**, 072303 (2003) 308, 309
144. S.S. Adler et al. [PHENIX Collaboration]: Phys. Rev. Lett. **98**, 172302 (2007) 308, 309
145. R. Vogt: Phys. Rev. **C 71**, 054902 (2005) 308, 309
146. V. Guzey, M. Strikman and W. Vogelsang: Phys. Lett. **B 603**, 173 (2004) 308, 309
147. K.J. Eskola, V.J. Kolhinen and C.A. Salgado: Eur. Phys. J. **C 9**, 61 (1999) 308, 309
148. A. Accardi, F. Arleo, W.K. Brooks, D. d'Enterria and V. Muccifora: Riv. Nuovo Cim. (2009), to appear; arXiv:0907.3534 [nucl-th] 308, 320
149. J.W. Cronin, H.J. Frisch, M.J. Shochet, J.P. Boymond, R. Mermod, P.A. Piroué and R.L. Sumner: Phys. Rev. **D 11**, 3105 (1975) 308
150. D. Antreasyan, J.W. Cronin, H.J. Frisch, M.J. Shochet, L. Kluberg, P.A. Piroué and R.L. Sumner: Phys. Rev. **D 19**, 764 (1979) 308
151. J. Adams et al. [STAR Collaboration]: Phys. Lett. **B 637**, 161 (2006) 308, 318
152. A. Adare et al. [PHENIX Collaboration]: Phys. Rev. **D 76**, 051106 (2007) 309, 310
153. S.S. Adler et al. [PHENIX Collaboration]: Phys. Rev. Lett. **91**, 072301 (2003) 310, 313
154. S.S. Adler et al. [PHENIX Collaboration]: Phys. Rev. Lett. **96**, 202301 (2006) 310, 311
155. S.S. Adler et al. [PHENIX Collaboration]: Phys. Rev. **C69**, 034910 (2004) 310
156. S.S. Adler et al. [PHENIX Collaboration]: Phys. Rev. Lett. **94**, 232301 (2005) 310, 311
157. B. Muller: Phys. Rev. **C 67**, 061901 (2003) 310
158. S.S. Adler et al. [PHENIX Collaboration]: Phys. Rev. **C 76**, 034904 (2007) 310, 316, 317
159. A. Adare et al. [PHENIX Collaboration]: arXiv:0804.4168 [nucl-ex] 311
160. I. Vitev and M. Gyulassy: Phys. Rev. Lett. **89**, 252301 (2002) 310, 311, 313, 314, 315
161. I. Vitev: J. Phys. **G 30**, S791 (2004) 310, 311, 313, 314, 315
162. A. Adare et al. [PHENIX Collaboration]: Phys. Rev. **C 77**, 064907 (2008) 310, 311
163. D. Molnar and M. Gyulassy: Nucl. Phys. **A 697**, 495 (2002) 312
164. D. Molnar and M. Gyulassy: Nucl. Phys. **A 703** (2002) 893 [Erratum] 312
165. S.A. Bass et al.: arXiv:0808.0908 [nucl-th] 312
166. S.S. Adler et al. [PHENIX Collaboration]: Phys. Rev. **C 71**, 034908 (2005) 313, 314, 326
167. S.S. Adler et al. [PHENIX Collaboration]: Phys. Rev. **C 71**, 049901 (2005) [Erratum] 313, 314, 326
168. M.M. Aggarwal et al. [WA98 Collaboration]: Eur. Phys. J. **C 23**, 225 (2002) 313, 315
169. D. d'Enterria: Phys. Lett. **B 596**, 32 (2004) 313, 314, 315

170. H. Buesching: Eur. Phys. J. **C 49**, 41 (2006) 313
171. I. Vitev: Phys. Lett. **B 606**, 303 (2005) 313, 314
172. M.M. Aggarwal et al. [WA98 Collaboration]: Phys. Rev. Lett. **100**, 242301 (2008) 314
173. S. Jeon, J. Jalilian-Marian and I. Sarcevic: Phys. Lett. **B 562**, 45 (2003) 314
174. B. Alessandro et al. [ALICE Collaboration]: J. Phys. **G 32**, 1295 (2006) 315, 328, 329
175. N. Grau [ATLAS Collaboration]: J. Phys. **G 35**, 104040 (2008) 315
176. D. d'Enterria et al. (eds.) [CMS Collaboration]: J. Phys. **G 34**, 2307 (2007) 315, 329
177. I. Vitev: Phys. Lett. **B 639**, 38 (2006) 315
178. A. Adare et al. [PHENIX Collaboration]: Phys. Rev. Lett. **101**, 162301 (2008) 315, 316
179. K. Reygers [PHENIX Collaboration]: J. Phys. **G 35**, 104045 (2008) 315, 316
180. V.S. Pantuev: JETP Lett. **85**, 104 (2007) 317
181. D. d'Enterria: Eur. Phys. J. **C 43**, 295 (2005) 317, 318
182. Q. Wang and X.N. Wang: Phys. Rev. **C 71**, 014903 (2005) 317, 318
183. B. Mohanty [STAR Collaboration]: J. Phys. **G 35**, 104006 (2008) 318
184. I. Vitev: J. Phys. **G 35**, 104011 (2008) 318, 319
185. R.C. Hwa and C.B. Yang: Phys. Rev. **C 67**, 034902 (2003) 318
186. R.J. Fries, B. Muller, C. Nonaka and S.A. Bass: Phys. Rev. **C 68**, 044902 (2003)
187. V. Greco, C.M. Ko and P. Levai: Phys. Rev. Lett. **90**, 202302 (2003) 318
188. S.S. Adler et al. [PHENIX Collaboration]: Phys. Rev. Lett. **96**, 032301 (2006) 319
189. A. Adare et al. [PHENIX Collaboration]: Phys. Rev. Lett. **98**, 172301 (2007)
190. B.I. Abelev et al. [STAR Collaboration]: Phys. Rev. Lett. **98**, 192301 (2007) 319
191. M. Djordjevic, M. Gyulassy and S. Wicks: Phys. Rev. Lett. **94**, 112301 (2005) 319
192. N. Armesto, A. Dainese, C. Salgado and U. Wiedemann: Phys. Rev. **D 71**, 054027 (2005) 319
193. Y. Morino [PHENIX Collaboration]: J. Phys. **G 35**, 104116 (2008) 319
194. A. Mischke [STAR Collaboration]: J. Phys. **G 35**, 104117 (2008) 319
195. M. Cacciari, P. Nason and R. Vogt: Phys. Rev. Lett. **95**, 122001 (2005) 319
196. A. Adil and I. Vitev: Phys. Lett. **B 649**, 139 (2007) 319, 320
197. M.G. Mustafa: Phys. Rev. **C 72**, 014905 (2005) 319
198. M. Djordjevic: Phys. Rev. **C 74**, 064907 (2006) 319
199. S. Caron-Huot and G.D. Moore: JHEP **0802**, 081 (2008) 319
200. H. van Hees, M. Mannarelli, V. Greco and R. Rapp: Phys. Rev. Lett. **100**, 192301 (2008) 320
201. P.R. Sorensen and X. Dong: Phys. Rev. **C 74**, 024902 (2006) 320
202. G. Martinez-Garcia, S. Gadrat and P. Crochet: Phys. Lett. **B 663**, 55 (2008) 320
203. C. Adler et al. [STAR Collaboration]: Phys. Rev. Lett. **90**, 082302 (2003) 320, 321, 322
204. J. Adams et al. [STAR Collaboration]: Phys. Rev. Lett. **95**, 152301 (2005) 321
205. S.S. Adler et al. [PHENIX Collaboration]: Phys. Rev. Lett. **97** 052301 (2006) 320, 321, 323
206. N.N. Ajitanand et al.: Phys. Rev. **C 72**, 011902 (2005) 320
207. J. Jia: arXiv:0810.0051 [nucl-ex] 321
208. A. Adare et al. [PHENIX Collaboration]: Phys. Rev. **C 77**, 011901 (2008) 321
209. A. Adare et al. [PHENIX Collaboration]: Phys. Rev. **C 78**, 014901 (2008) 321, 322, 323, 324
210. M.J. Tannenbaum: Int. J. Mod. Phys. **E 16**, 2011 (2007) 321
211. H. Zhang, J.F. Owens, E. Wang and X.N. Wang: Phys. Rev. Lett. **98**, 212301 (2007) 322
212. J. Adams et al. [STAR Collaboration]: Phys. Rev. Lett. **97**, 162301 (2006) 322
213. M.J. Horner [STAR Collaboration]: J. Phys. **G 34**, S995 (2007) 323
214. A.D. Polosa and C.A. Salgado: Phys. Rev. **C 75**, 041901 (2007) 323
215. J.G. Ulery: J. Phys. **G 35**, 104032 (2008) 324
216. B.I. Abelev et al. [STAR Collaboration]: arXiv:0805.0622 [nucl-ex] 324
217. N.N. Ajitanand [PHENIX Collaboration]: Nucl. Phys. **A 783**, 519 (2007) 324
218. S.S. Gubser, S.S. Pufu and A. Yarom: Phys. Rev. Lett. **100**, 012301 (2008) 324
219. P.M. Chesler and L.G. Yaffe: Phys. Rev. **D 78**, 045013 (2008) 324
220. R.B. Neufeld, B. Muller and J. Ruppert: Phys. Rev. **C 78**, 041901 (2008) 324
221. H. Stoecker: Nucl. Phys. **A 750**, 121 (2005) 324
222. J. Casalderrey-Solana, E.V. Shuryak and D. Teaney: Nucl. Phys. **A 774**, 577 (2006)

223. B. Betz, M. Gyulassy, D.H. Rischke, H. Stocker and G. Torrieri: J. Phys. **G 35**, 104106 (2008) 324
224. B. Betz, J. Noronha, G. Torrieri, M. Gyulassy, I. Mishustin and D.H. Rischke: arXiv:0812.4401 [nucl-th] 324
225. J. Noronha, M. Gyulassy, and G. Torrieri: arXiv:0807.1038 [hep-ph]
226. M. Gyulassy, J. Noronha and G. Torrieri: arXiv:0807.2235 [hep-ph]
227. B. Betz, M. Gyulassy, J. Noronha and G. Torrieri: arXiv:0807.4526 [hep-ph] 325
228. R.B. Neufeld: Phys. Rev. **D 78**, 085015 (2008)
229. R.B. Neufeld: arXiv:0810.3185 [hep-ph] 324
230. J. Putschke: J. Phys. **G 34**, S679 (2007) 325
231. M. van Leeuwen [STAR collaboration]: arXiv:0808.4096 [nucl-ex] 325
232. C.A. Pruneau, S. Gavin and S.A. Voloshin: Nucl. Phys. **A 802**, 107 (2008) 325
233. A. Dumitru, F. Gelis, L. McLerran and R. Venugopalan: Nucl. Phys. **A 810**, 91 (2008) 325
234. B. Alver et al. [PHOBOS Collaboration]: J. Phys. **G 35**, 104080 (2008) 325
235. S.D. Ellis, J. Huston, K. Hatakeyama, P. Loch and M. Tonnesmann: Prog. Part. Nucl. Phys. **60**, 484 (2008) 326, 327
236. C. Buttar et al.: arXiv:0803.0678 [hep-ph] 326, 327
237. S. Catani, Y.L. Dokshitzer, M.H. Seymour and B.R. Webber: Nucl. Phys. **B 406**, 187 (1993) 326
238. G.P. Salam and G. Soyez: JHEP **0705**, 086 (2007) 326
239. M. Cacciari and G.P. Salam: Phys. Lett. **B 641**, 57 (2006) 326, 328
240. M. Cacciari and G.P. Salam: Phys. Lett. **B 659**, 119 (2008) 326, 329
241. M. Cacciari, G.P. Salam and G. Soyez: JHEP **0804**, 005 (2008) 328, 329
242. A. Morsch [ALICE Collaboration]: AIP Conf. Proc. **1026**, 72 (2008) 326, 333
243. S.L. Blyth et al.: J. Phys. **G 34**, 271 (2007) 326
244. O. Kodolova, I. Vardanian, A. Nikitenko and A. Oulianov: Eur. Phys. J. **C 50**, 117 (2007) 326, 329
245. M. Cacciari, G.P. Salam and G. Soyez: JHEP **0804**, 063 (2008) 327, 328
246. S.D. Ellis and D.E. Soper: Phys. Rev. **D 48**, 3160 (1993) 328
247. M. Wobisch and T. Wengler: arXiv:hep-ph/9907280 328
248. M. Gyulassy and X.N. Wang: Comput. Phys. Commun. **83**, 307 (1994) 329
249. J. Putschke [STAR Collaboration]: Eur. Phys. J. **C 61**, 629 (2009), arXiv:0809.1419 329
250. S. Salur [STAR Collaboration]: arXiv:0810.0500 [nucl-ex] 329
251. G.L. Bayatian et al. [CMS Collaboration]: J. Phys. **G 34**, 995 (2007) 329, 330
252. M. Dasgupta, L. Magnea and G.P. Salam: JHEP **0802**, 055 (2008) 330
253. D.E. Acosta et al. [CDF Collaboration]: Phys. Rev. **D 71**, 112002 (2005) 331
254. Y.L. Dokshitzer, V.A. Khoze, A.H. Mueller and S.I. Troian: *Basics of Perturbative QCD*, p. 274, Ed. Frontières, Gif-sur-Yvette, France (1991) 331
255. Y.I. Azimov, Y.L. Dokshitzer, V.A. Khoze and S.I. Troyan: Z. Phys. **C 27**, 65 (1985) 332
256. N. Borghini: Eur. Phys. J. **C 49**, 327 (2007) 332
257. X.N. Wang, Z. Huang and I. Sarcevic: Phys. Rev. Lett. **77**, 231 (1996) 332
258. G. Conesa, H. Delagrangé, J. Diaz, Y.V. Kharlov and Y. Schutz: Nucl. Instrum. Meth. **A 585**, 28 (2008) 333
259. C. Loizides [CMS Collaboration]: J. Phys. **G 35**, 104166 (2008) 333